Structural Alignments of (+)- and (−)-*trans-anti*-Benzo[a]pyrene-dG Adducts Positioned at a DNA Template−Primer Junction†

Monique Cosman,‡ Brian E. Hingerty,§ Nicholas E. Geacintov,|| Suse Broyde,⊥,# and Dinshaw J. Patel*,‡

Cellular Biochemistry and Biophysics Program, Memorial Sloan Kettering Cancer Center, New York, New York 10021, Health Sciences Research Division, Oak Ridge National Laboratory, Oak Ridge, Tennessee 37831, and Chemistry and Biology Departments, New York University, New York, New York 10003

Received June 30, 1995; Revised Manuscript Received September 25, 1995⊗

ABSTRACT: The structural features of a chemically modified DNA template strand may promote error-prone DNA synthesis during replication. The resulting higher incidence of mutations, in turn, can eventually lead to tumor initiation. Structural insights into this process can be monitored by studying chemically modified base adducts of defined stereochemistry positioned site-specifically at a single strand−duplex template−primer junction. We have used a NMR-molecular mechanics approach to obtain the solution conformations of the covalent adducts derived from *trans* additions at the [BP]C[10] position of the highly tumorigenic (+)-*anti*-benzo[*a*]pyrene diol epoxide [(+)-*anti*-BPDE] and nontumorigenic (−)-*anti*-benzo-[a]pyrene diol epoxide [(−)-*anti*-BPDE] to the N^2 position of guanine [(+) and (−)-*trans-anti*-[BP]dG, respectively] in the d(A1-A2-C3-[BP]G4-C5-T6-A7-C8-C9-A10-T11-C12-C13)·d(G14-G15-A16-T17-G18-G19-T20-A21-G22) 13/9-mer DNA sequence. The modified 13-mer strand constitutes the template strand, while the complementary 9-mer strand constitutes a primer which has been synthesized from the 3′-end of the template toward the 5′-end up to the base preceding, but not including, the modified guanine. The modified guanine (denoted by [BP]dG4) is positioned at the junction site between the single-stranded and duplex segments. Structural features of the (+)-*trans-anti*-[BP]dG 13/9-mer have been determined by incorporating proton−proton distances defined by lower and upper bounds deduced from NOESY spectra as restraints in molecular mechanics computations in torsion angle space. The 3′-side duplex segment retains a minimally perturbed B-DNA conformation with all nine base pairs in Watson−Crick hydrogen-bonded alignments. Conformational heterogeneity is detected at the single-stranded d(A1-A2-C3) segment located 5′ to the modified (+)-*trans-anti*-[BP]dG lesion which contrasts with an unperturbed alignment of these same residues in the unmodified control 13/9-mer. The modified guanine adopts a *syn* glycosidic torsion angle, is displaced into the major groove, and no longer stacks over the adjacent dC5·dG22 base pair. Such a base displacement is accompanied by stacking of one face of the pyrenyl ring with the dC5·dG22 base pair located on the duplex segment proximate to the modified guanine, while the other face of BP is exposed to solvent. The orientations elucidated for the modified guanine and benzo[a]pyrenyl rings in the (+)-*trans-anti*-[BP]dG template−primer junction contrasts with orientations previously reported for the same adduct when positioned opposite either a dC base [Cosman, M., et al. (1992) *Proc. Natl. Acad. Sci. U.S.A. 89,* 1914−1918] or a deletion site [Cosman, M., et al. (1994) *Biochemistry 33,* 11507−11517] at the duplex level. The NMR spectra of the stereoisomeric (−)-*trans-anti*-[BP]dG 13/9-mer are characterized by very broad and overlapped resonances for the protons located at the lesion site and for the single-strand and duplex segments flanking this site as well as by the presence of exchange cross peaks. This result indicates conformational heterogeneity for the strand and duplex segments on either side of the lesion site in the (−)-*trans-anti*-[BP]dG 13/9-mer precluding characterization of the structural alignment of this lesion when positioned at the template−primer junction. The different spectral and structural patterns associated with the stereoisomeric (+)- and (−)-*trans-anti*-[BP]dG 13/9-mers should help to define the interrelationship between the conformations of site-specific and stereochemically defined covalent DNA adducts at template−primer junction sites and their effects on the action of polymerases in the cell.

Polynuclear aromatic hydrocarbons (PAHs) are ubiquitous environmental pollutants, which can be metabolically activated by cellular P-450 enzymes to electrophilic diol epoxide derivatives (Sims & Grover, 1974; Miller, 1978; Gelboin, 1980; Conney, 1982). These highly reactive metabolites can, in turn, bind covalently to cellular DNA [reviewed in Singer and Grunberger (1983)]. Two of the metabolically activated derivatives of benzo[a]pyrene (BP), one of the most widely studied PAH compounds (Phillips, 1987), are the enantiomeric 7*R*,8*S*-dihydroxy-9*S*,10*R*-epoxybenzo[a]pyrene [(+)-*anti*-BPDE) and 7*S*,8*R*-dihydroxy-9*R*,10*S*-epoxybenzo[a]-pyrene [(−)-*anti*-BPDE] (Sims et al., 1974), each of which display striking differences in their biological activities (Levin et al., 1976; Wood et al., 1977; Kapitulnik et al., 1978; Stevens et al., 1985). While (+)-*anti*-BPDE is highly

† This research is supported by NIH Grant CA-46533 to D.J.P., by NIH CA-20851 and DOE Grant DE-FG02-88ER60405 to N.E.G., by NIH Grant CA-28038, NIH Grant RR-06458, and DOE Grant DE-FG02-90ER60931 to S.B., and by DOE Contract DE-AC05-840R21400 with Martin-Marietta Energy Systems and DOE OHER Field Work Proposal ERKP931 to B.E.H.

‡ Memorial Sloan Kettering Cancer Center.
§ Oak Ridge National Laboratory.
|| Chemistry Department, New York University.
⊥ Biology Department, New York University.
The coordinates are available from Dr. Suse Broyde, who can be contacted by E-mail at broyde@acfcluster.nyu.edu.

⊗ Abstract published in *Advance ACS Abstracts,* November 1, 1995.

0006-2960/95/0434-15334$09.00/0

tumorigenic in mice, (−)-*anti*-BPDE is not (Levin et al., 1976; Kapitulnik et al., 1978). In addition, early studies showed that the (+)-enantiomer is more mutagenic in mammalian cells than the (−)-enantiomer (Wood et al., 1977; Brookes & Osborne, 1982; Stevens et al., 1985). However, in bacterial cells, the reverse trend is observed in that (−)-*anti*-BPDE was more active than the (+)-enantiomer (Wood et al., 1977; Stevens et al., 1985).

Both (+)- and (−)-*anti*-BPDE enantiomers bind predominantly to the N^2 position of guanine (N^2-dG) by *trans* addition at the C^{10} carbon of BPDE (Osborne et al., 1976; Jeffrey et al., 1976; Meehan & Straub, 1979; Cheng et al., 1989). Minor products can also be obtained at the N^2-dG position by *cis* addition, as well as by *trans* and *cis* additions at the N^7 position of guanine and at the exocyclic N^6 amino group of adenine (Weinstein et al., 1976; Jeffrey, 1985; Meehan & Straub, 1979; Cheng et al., 1989).

Wei et al. (1993, 1994) compared the mutation spectra induced by either (+)- or (−)-*anti*-BPDE binding to the *HPRT* locus in Chinese hamster V-79 cells. Consistent with the earlier data in mammalian cells (Wood et al., 1977; Brookes & Osborne, 1982; Stevens et al., 1985), the (+)-isomer was found to be more mutagenic than the (−)-enantiomer. Both (+)- and (−)-*anti*-BPDE induced predominantly dG·dC → dT·dA transversions and other base substitution mutations, followed by exon deletions and frameshifts. Rodriguez and Loechler (1993) studied the mutation specificity caused by the binding of (+)-*anti*-BPDE to a *supF* gene in an *Escherichia coli* plasmid (pUB3) and found that the most frequently observed point mutations are also dG·dC → dT·dA transversions. The advantage of using (+)- or (−)-*anti*-BPDE enantiomers rather than racemic-*anti*-BPDE in these studies is that fewer adduct types need be considered in interpreting the mutation spectra; however, effects due to stereochemically defined *trans* and *cis* adducts situated at specific sites could not be distinguished unambiguously in these studies.

The availability of site-specifically modified deoxyoligonucleotides with stereochemically defined *anti*-BPDE-dG lesions has facilitated studies of *in vitro* transcription (Choi et al., 1994) and *in vitro* polymerase-catalyzed primer extension reactions (Hruszkewycz et al., 1992; Shibutani et al., 1993) using BPDE-modified oligonucleotides as templates. Hruszkewycz et al. (1992) showed that (+)-*anti*-BPDE-dG lesions are bypassed by Sequenase (Version 2.0) and human polymerase α only with great difficulty; when the lesion was bypassed, the normal deoxycytosine residue was incorporated opposite the modified deoxyguanosyl residue in the fully extended primer. Shibutani et al. (1993) used stereochemically defined and site-specific *trans* and *cis*-N^2-dG deoxyoligonucleotide adducts derived from both (+)- and (−)-*anti*-BPDE as templates in primer extension reactions catalyzed by the Klenow fragment of *E. coli* DNA polymerase I. While primer extension was strongly blocked by each of the stereochemically distinct (+)- and (−)-*trans* and *cis*-*anti*-[BP]dG lesions, small amounts of dAMP were incorporated opposite the lesion, and one- and two-base deletions were also found in the extended primers. The *trans* and *cis* lesions derived from the (−)-*anti*-BPDE enantiomer were found to have higher miscoding potentials than those derived from the (+)-*anti* isomer. Choi et al. (1994) found that site-specific (+)- and (−)-*trans* and *cis*-*anti*-[BP]dG lesions inhibit transcription elongation by bacteriophage T7 RNA polymerase in the order (+)-*trans* > (−)-*trans* > (+)-*cis* > (−)-*cis*. In site-directed mutagenesis experiments with double-stranded plasmids containing single, site-specifically placed (+)-*trans*-*anti*-[BP]dG lesions transfected in *E. coli*, the principal observed mutations are dG·dC → dT·dA transversions (Mackay et al., 1992). Moriya et al. (1995) have also used a site-specific approach to study the mutagenic potentials of both (+)- and (−)-*trans*-*anti*-[BP]dG lesions; these were positioned within codons 60 and 61 of the noncoding strand of the human *c-Ha-ras* protooncogene sequence in a single-stranded shuttle vector introduced into *E. coli* or simian kidney (COS) cells. When the lesion was bypassed, the (+)- or (−)-*trans*-*anti*-[BP]dG adducts were found to preferentially pair to dCMP and dAMP.

Thus, the structural features of unrepaired site-specific and stereochemically defined BPDE-DNA lesions can block polymerases and induce errors in DNA or RNA synthesis during replication or transcription. A systematic study of the interrelationship between the structures of site-specific and stereochemically defined covalent DNA adducts and their effects on the actions of polymerases should further our understanding of the mechanisms of PAH induced carcinogenesis and mutagenesis at the molecular level.

Previously, we had elucidated the solution structures of both the (+)- and (−)-*trans*-*anti*-[BP]dG·dC 11-mer duplexes in the sequence d(C-C-A-T-C-[BP]G-C-T-A-C-C)·d(G-G-T-A-G- C-G-A-T-G-G) (Cosman et al., 1992; de los Santos et al., 1992). In the structures of both (+)- and (−)-*trans*-*anti*-[BP]dG duplex adducts, the covalently attached benzo[a]pyrenyl moieties are located in a widened minor groove of a minimally perturbed B-DNA helix with one face of the aromatic pyrenyl ring system stacking over the sugar residues of the unmodified complementary strand, while the other face is solvent exposed. However, the long axis of the pyrenyl ring is oriented toward the 5′-end of the modified strand in the (+)-*trans* isomer (Cosman et al., 1992; Fountain & Krugh, 1995) and in the opposite direction toward the 3′-end in the (−)-*trans* isomer duplex (de los Santos et al., 1992).

In addition, we have obtained the solution structure of the (+)-*trans*-*anti*-[BP]dG·del duplex adduct in the sequence d(C-C-A-T-C-[BP]G-C-T-A-C-C)·d(G-G-T-A-G-G-A-T-G-G) (Cosman et al., 1994) in order to gain a better understanding of the structural basis for the deletions observed in the mutational spectra obtained in studies of DNA covalently modified by (+)-*anti*-BPDE (Wei et al., 1993; Shibutani et al., 1993). Eliminating the partner cytosine opposite the modified guanine resulted in a dramatic change in the positions of both the modified guanine and the attached benzo[a]pyrenyl moiety relative to the surrounding DNA residues. The modified guanine is displaced into the major groove and stacks over the major groove base protons of the 5′-side cytosine, all remaining 10 base pairs are Watson−Crick hydrogen bonded, and the benzo[a]pyrenyl moiety intercalates between flanking intact dG·dC base pairs.

In the present work, we have used two-dimensional NMR techniques in conjunction with molecular mechanics calculations to define structural features of (+) and (−)-*trans*-*anti*-[BP]dG adducts (**1** and **2**) located at the junction site of a single-strand/duplex 13/9-mer sequence **3**, which models a template−primer junction. The modified 13-mer strand mimics the template strand, while the complementary 9-mer strand simulates a primer which extends from the 3′-end of

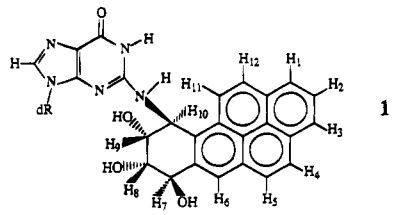

1

(+)-*trans-anti*-[BP]dG

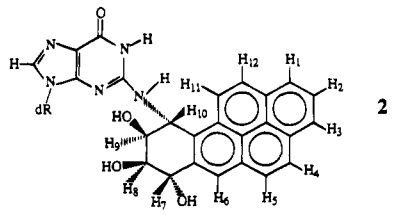

2

(-)-*trans-anti*-[BP]dG

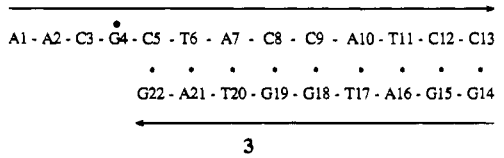

3

the template strand toward the 5′-end up to the base preceding, but not including, the modified guanine.

MATERIALS AND METHODS

Preparation of the (+)- and (−)-trans-anti-[BP]-dG 13/9-Mers. Racemic *anti*-BPDE was purchased from the National Cancer Center Institute Chemical Carcinogen Reference Standard Repository. The syntheses of the (+)- and (−)-*trans-anti*-BP-N^2-dG covalent adducts in the d(A-A-C-[BP]G-C-T-A-C-C-A-T-C-C) sequence were carried out using previously described methods (Cosman et al., 1990) starting, however, with (±)-*anti*-BPDE. The (+)-*trans*-, (−)-*trans*, (+)-*cis*, and (−)-*cis-anti*-[BP]dG isomeric covalent adducts at the 13-mer strand level were separable by preparative HPLC on a C18 ODS Hypersil column (Cosman et al., 1990). The enantiomerically pure modified (+)- and (−)-*trans-anti*-[BP]dG 13-mer d(A-A-C-[BP]G-C-T-A- C-C-A-T-C-C) strands were annealed to the complementary unmodified 9-mer d(G-G-A-T-G-G- T-A-G) strands at 70 °C, and the stoichiometry was followed by monitoring single proton resonances in both strands.

NMR Experiments. A combination of through-space nuclear Overhauser effect (NOESY) and through-bond correlated (COSY, TOCSY) two-dimensional spectra were recorded on approximately 6.7 mg of the unmodified control 13/9-mer, 9.9 mg of the (+)-*trans-anti*-[BP]dG 13/9-mer, and 6.7 mg of the (−)-*trans-anti*-[BP]dG 13/9-mer in 0.6 mL of 0.1 M NaCl, 10 mM phosphate, pH 7.0, aqueous buffer and analyzed in order to assign the carcinogen and nucleic acid protons. All experiments were carried out using a Varian Unity Plus 600 MHz instrument in the States-TPPI mode (Marion et al., 1989) with a 2.0 s relaxation delay between scans. The temperature of the samples was calibrated with an external methanol sample. NOESY spectra (150 ms mixing time) of the unmodified control and (−)-*trans-anti*-[BP]dG 13/9-mers at pH 7.0 and of the (+)-*trans-anti*-[BP]dG 13/9-mer at pH 7.0 and 5.7 in H_2O buffer at 1 °C were collected using a jump−return pulse for solvent suppression.

NOESY spectra (50 and 300 ms mixing times) were recorded for the unmodified control 13/9-mer at 25 °C and for the (+)-*trans-anti*-[BP]dG 13/9-mer in D_2O buffer at 10, 25, and 29 °C. NOESY data sets (50, 90, 130, 170, 210, and 300 ms mixing times) at 25 °C were obtained for both (+)- and (−)-*trans-anti*-[BP]dG 13/9-mers in D_2O buffer at 25 °C. The through-bond TOCSY data sets for the unmodified control and (−)-*trans-anti*-[BP]dG 13/9-mers in D_2O buffer were recorded at spin lock times of 40 and 80 ms at 25 °C and for the (+)-*trans- anti*-[BP]dG 13/9-mer at spin lock times of 40, 60, and 80 ms at 10, 25, and 29 °C.

The proton−phosphorus correlation spectra of the unmodified control and (−)-*trans-anti*-[BP]dG 13/9-mers were recorded at 25 °C and of the (+)-*trans-anti*-[BP]dG 13/9-mer at 25 and 29 °C, in D_2O buffer, pH 7.0, using the method described in Sklenar et al. (1986) with sweep widths set to 6 ppm in both ω_1 and ω_2, and with a 1.3 s presaturation of the HDO signal. The phosphorus spectra were referenced with an external 10% (v/v) trimethylphosphate (TMP) sample. A proton−carbon HMQC correlation spectrum on the (+)-*trans-anti*-[BP]dG 13/9-mer was recorded in D_2O buffer, pH 7.0, at 25 °C. The proton carrier frequency was set to 4.5 ppm with a sweep width of 8.5 ppm, while the ^{13}C carrier frequency was set to 67.0 ppm with a sweep width of 66.0 ppm. The carbon spectra were referenced relative to external 3-(trimethylsilyl)propionate (TSP) using the method described by Bax and Subramanian (1986).

Several factors went into the conversion of the NOE intensities into the distance bounds used for the structure determination of the adduct 13/9-mers. Distance restraints involving nonexchangeable protons were estimated from NOE buildup curves of NOESY spectra recorded at 50, 90, 130, 170, and 210 ms on the adduct 13/9-mers in D_2O if the corresponding cross peaks were reasonably well resolved and not too broad. The interproton distance calculations were based on the isolated two-spin approximation using the dT(NH3)−dA(H2) fixed distance of 2.92 Å for the NOESY spectra in H_2O and the dC(H6)−dC(H5) fixed distance of 2.45 Å for the NOESY data sets in D_2O solution. The choice of upper and lower bound ranges on the estimated distances depended on the resolution of the cross peaks in the contour plots. However, the cross peaks between protons located at or close to the lesion site in the adduct 13/9-mers were broad, overlapped, and exhibited exchange cross peaks. In these cases, the distance restraints were estimated from counting the number of NOE cross peak contours present at both short (50 ms) and long (300 ms) mixing times and given as strong (2.2−3.5 Å), medium (3.0−4.5 Å), and weak (4.0−6.0 Å). The base proton to sugar H1′ NOE cross peaks in the shortest mixing time NOESY data set in D_2O were evaluated to qualitatively differentiate between *syn* (strong NOE) and *anti* (weak NOE) glycosidic torsion angles (Patel et al., 1982).

The proton−proton vicinal coupling constants among sugar protons were analyzed from phase-sensitive COSY spectra to qualitatively distinguish between the C3′-*endo* and C2′-*endo* family of sugar puckers in the control, (+)-, and (−)-*trans-anti*-[BP]dG 13/9-mers. The relative intensity of the NOE cross peaks between base protons and their own and 5′-flanking sugar H2′, H2″, and H3′ protons were used to qualitatively distinguish between the A and B family of helices for the modified duplex (van der Ven & Hilbers, 1988).

Molecular Mechanics Computations of the (+)-trans-anti-[BP]dG 13/9-Mer. We employ our own molecular mechan-

ics program DUPLEX (Hingerty et. al., 1989), which has been especially tailored for investigating carcinogen−DNA adducts. One key feature of DUPLEX is that it employs a consistent force field for both the carcinogen and the DNA. The DNA force field is essentially one developed in the laboratory of Olson (Taylor & Olson, 1983), and all carcinogen parameters, including the partial charge set, are consistent with it. This allows the force field to play a part in an interactive way, as described below, in the modeling of the structure. Force field parameters, including partial charges, for the (+)-*trans-anti*-[BP]dG adduct were the same as those employed previously for the (+)-*trans-anti*-[BP]-dG•dC 11-mer duplex and (+)-*trans-anti*- [BP]dG•deletion duplex (Cosman et al., 1992, 1994) and for the (−)-*trans-anti*-[BP]dG adduct as in the (−)-*trans-anti*-[BP]dG•dC 11-mer duplex (de los Santos et al., 1992). The conformation of the benzylic ring was in the distorted half-chair form with the BP(H7) and BP(H8) protons in the diaxial domain and BP(H9) and BP(H10) protons in the diequatorial domain (Neidle et al., 1982).

In addition to the consistent force field, we employ special strategies to address the multiple minimum problem, which hinders locating the lowest energy structure on the potential energy surface. We employ energy minimization searches using the reduced variable domain of torsion angle space, also known as internal coordinates. In this approach, bond lengths, bond angles, and dihedral angles in aromatic rings, which vary little in nature, are kept fixed. The flexible torsion angles and the pseudorotation parameter, which can adopt any value from 0° to 360°, are the variables for energy minimization, rather than the *xyz*'s of Cartesian space. This approximation is suitable for investigating equilibrium structures. Thus, the number of variables that the minimization algorithm must simultaneously optimize is vastly reduced: from $3N - 6$ (where N is the number of atoms) to 9 in a carcinogen-modified nucleotide residue with two carcinogen−base torsion linkages. Consequently, the minimizer is much more powerful in locating low energy conformations, as the potential energy surface is much smoother. Furthermore, we study small modified subunits (which have fewer variables) first. The subunits that are in accord with the data are subsequently built to the full sized duplex by embedding or other building strategies that we have developed (Hingerty et al., 1989; Shapiro et al., 1989). The energy minimization searches of the carcinogen−DNA orientation space employ starting structures with arbitrary, unbiased high energy carcinogen−DNA orientations. Typically, the two carcinogen−DNA torsion angles are surveyed at 90° intervals of each, in combination, for a total of 16 trials in one set.

Penalty functions or pseudopotential energies (restraints) are employed as additions to the energy function, but only to guide the minimizer in the direction of the observed structure on the multidimensional hill and valley terrain of the potential energy surface. For restraints derived from NMR data, upper and lower bounds are included, using the following functions:

$$F_N = W_N \sum_1^n (d - d_N)^2 \quad (1)$$

$$F_{NN} = W_{NN} \sum_1^n (d - d_{NN})^2 \quad (2)$$

The W's are adjustable weights (in the range of 10−30 kcal/mol•Å^2), d is the current value of the interproton distance, d_N is a target upper bound, and d_{NN} is a target lower bound. The summation is over all n NMR-derived distance bounds. Equation 1 is implemented when d is greater than d_N, and eq 2 is implemented when d is less than d_{NN}. F_N and F_{NN} can also be employed as goodness-of-fit indices to compare the quality of computed structures with respect to the NMR data. Here the d values are the achieved distances in a given model, and the W's are the weights employed in the search. F_N and F_{NN} are composites, reflecting the overall fit of all the achieved distances to their targets. They both adopt values of zero when all model distances are within the upper and lower NMR distance bounds. An important aspect of our use of these functions is the assigned value for W. Its value is chosen so that the penalty function is not dominant. Rather, the potential energy is dominant. Thus, with an appropriate weight, the pseudopotentials contribute sufficiently to the energy function to guide the minimizer to target geometries without overwhelming the intrinsic potential energy.

DUPLEX features an additional unique hydrogen bond penalty function (Hingerty et al., 1989) that is extremely useful for locating structures with unusual hydrogen bonding patterns or denatured sites. The function can be employed to search for structures with any selected hydrogen bonding pattern or denaturation between any designated residues on either strand. Our search strategy employs a limited set of key NMR distance restraints (in the range of one dozen to several dozen), together with information from the NMR data on the hydrogen bonding pattern between bases for the hydrogen bond penalty function. NMR information about the glycosidic torsion angle and the deoxyribose sugar pseudorotation parameter can also be included. The resulting structures are ranked according to energy and goodness of fit (eqs 1 and 2). At this point the first set of NMR assigned distance bounds are evaluated in relation to achieved distances and energies in the ensemble of 16 structures. Especially in the case of conformational heterogeneity, this affords feedback to the NMR analysis and offers the opportunity for reassessment of the distance bounds. This procedure can be carried out interactively until structures of lowest energy and best goodness of fit are located. The structures with the best fit to the data are also usually among the lowest in energy. A family of such structures is usually found. Finally, the best subunit is built to the larger modified duplex with all restraints, and then all penalty functions are released to yield final unrestrained minimum energy structures in accord with the data. If final structures do not retain features consistent with the NMR data, further searches are performed.

Computations were carried out at the Department of Energy's National Energy Research Supercomputer Center and the National Science Foundation's San Diego Supercomputer Center.

RESULTS

Exchangeable Protons in the Control 13/9-Mer. The exchangeable imino proton NMR spectrum (9.5−14.5 ppm) of the unmodified control 13/9-mer in H_2O buffer solution, pH 7.0, at 1 °C is characterized by well resolved and narrow

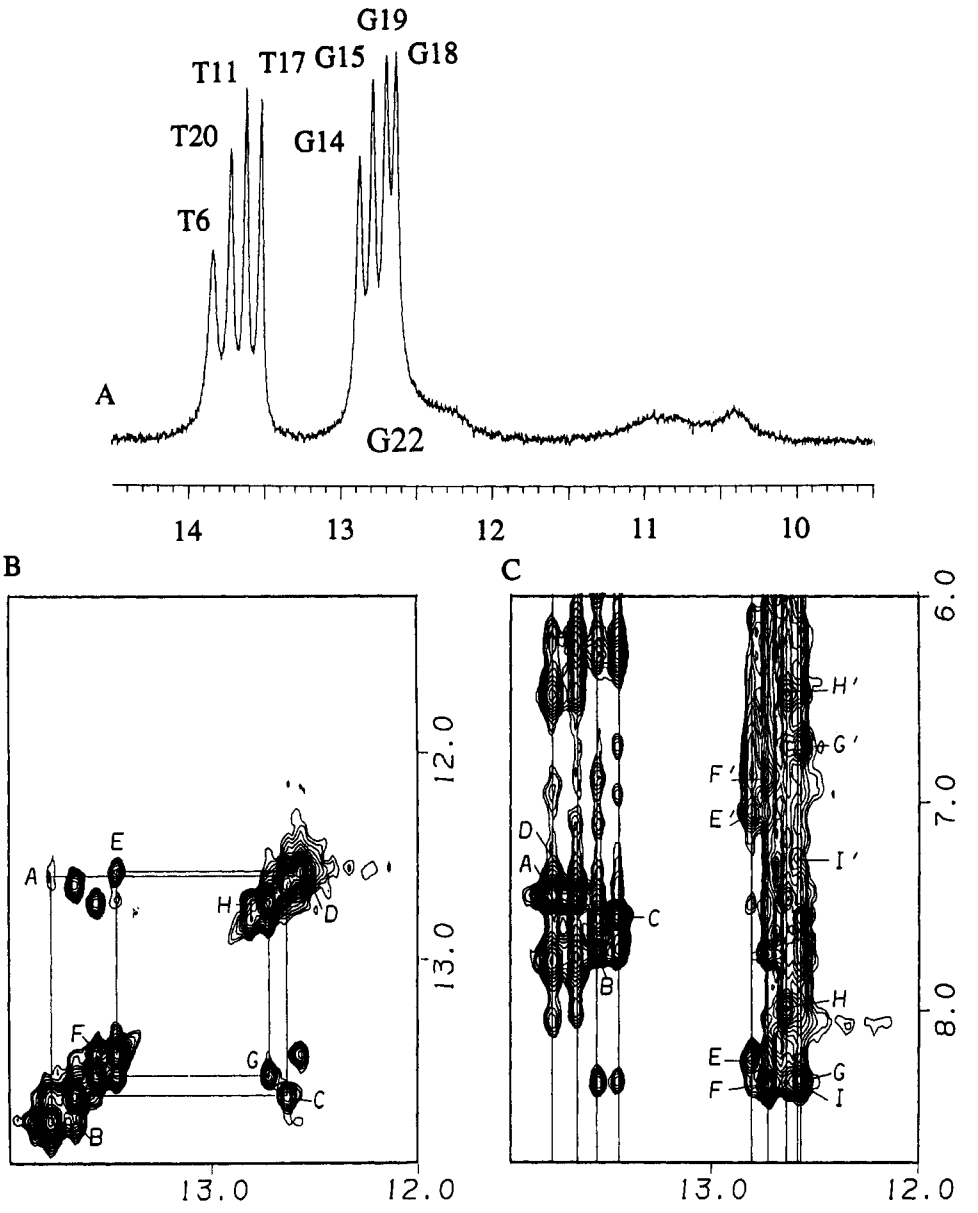

FIGURE 1: (A) Exchangeable imino proton spectrum (9.5−14.5 ppm) and (B) and (C) expanded NOESY (150 ms mixing time) contour plots of the control 13/9-mer in H_2O buffer at 1 °C. The imino proton assignments are recorded over the spectrum in panel A. NOE connectivities between adjacent base pairs in the symmetrical 12.0−14.2 ppm region are traced in panel B, starting at dG22 located at the duplex−single strand junction site and proceeding to dG14 toward the other end of the helix. The cross peaks A−H are assigned as follows: A, dG22(NH1)-dT6(NH3); B, dT6(NH3)-dT20(NH3); C, dT20(NH3)-dG19(NH1); D, dG19(NH1)-dG18(NH1); E, dG18(NH1)-dT17(NH3); F, dT17(NH3)-dT11(NH3); G, dT11(NH3)-dG15(NH1); H, dG15(NH1)-dG14(NH1). NOE connectivities between the imino protons (12.0−14.2 ppm) and the nucleic acid base and amino protons (6.0−8.7 ppm) are designated in panel C. The cross peaks A−I′ are assigned as follows: A, dT6(NH3)-dA21(H2); B, dT11(NH3)-dA16(H2); C, dT17(NH3)-dA10(H2); D, dT20(NH3)-dA7(H2); E,E′, dG14-(NH1)-dC13(NH_2-4b,e); F,F′, dG15(NH1)-dC12(NH_2-4b,e); G,G′, dG18(NH1)- dC9(NH_2-4b,e); H,H′, dG19(NH1)-dC8(NH_2-4b,e); I,I′, dG22(NH1)-dC5(NH_2-4b,e).

resonances between 12.5 and 14.0 ppm and very broad resonances between 10.4 and 10.8 ppm (Figure 1A). The imino proton assignments were determined following analysis of the 150 ms mixing time NOESY spectrum of the control 13/9-mer in H_2O buffer, pH 7.0, at 1 °C using standard procedures [reviewed in Patel et al. (1987) and van de Ven and Hilbers (1988)]. The connectivity between imino protons of adjacent base pairs in the d(C5-T6-A7-C8-C9-A10-T11-C12-C13)·d(G14-G15-A16-T17-G18-G19-T20-A21-G22) duplex segment can be traced from dC13·dG14 pair located at one end of the helix to the dC5·dG22 pair located at the opposite end proximate to the strand/duplex junction in the expanded NOESY plot of the symmetrical 12.0−14.0 ppm region (solid line, Figure 1B). Note, however, that the cross peak intensity between the imino protons of T6 and G22 is weak (peak A, Figure 1B).

An expanded NOESY contour plot of the control 13/9-mer correlating the NOEs between the imino protons (12.0−14.0 ppm) and the base and amino protons (6.0−8.7 ppm) is plotted in Figure 1C. Watson−Crick pairing in the 9-mer duplex segment is established at all four dA·dT pairs by the presence of a characteristic NOE between the thymine imino and adenine H2 protons across the pair (peaks A−D, Figure 1C) and at all five dG·dC pairs, including the terminal dC5·dG22 base pair located near the strand/duplex junction, by the presence of the characteristic NOEs between the guanine imino and cytosine amino protons across the pair (peaks E-I and E′-I′, Figure 1C).

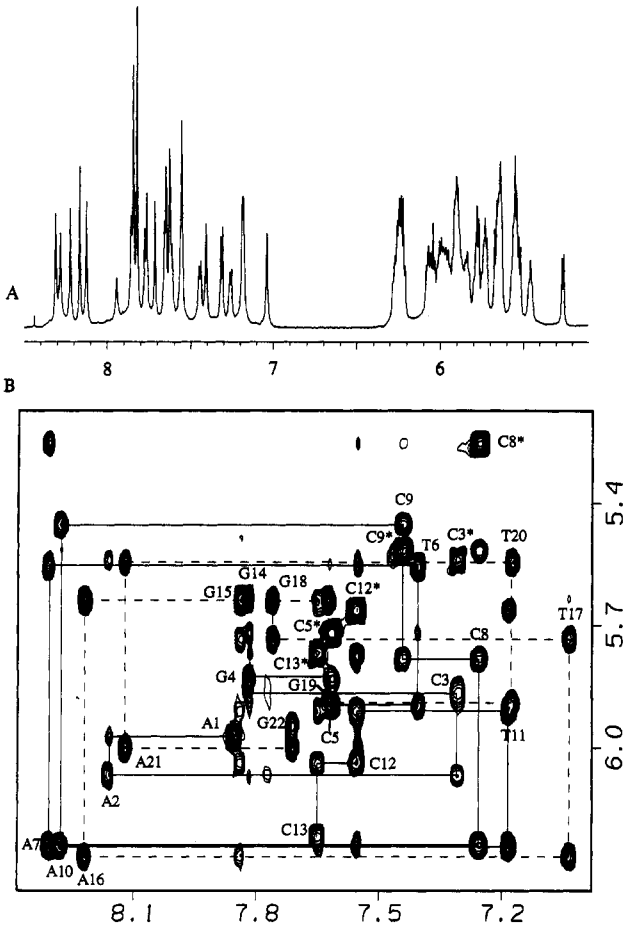

FIGURE 2: (A) Nonexchangeable proton spectrum (5.1−8.5 ppm) and (B) expanded NOESY (300 ms mixing time) contour plot of the control 13/9-mer in D_2O buffer at 25 °C, establishing distance connectivities between the base (purine H8 and pyrimidine H6) protons (7.0−8.4 ppm) and the sugar H1′ and cytosine H5 protons (5.2−6.4 ppm). The NOE connectivities between the bases (7.0−8.4 ppm) and their own and 5′-flanking sugar H1′ protons are traced from dA1 to dC13 on the template strand (solid line) and from dG14 to dG22 on the primer strand (dashed line). The cross peaks between cytosine H5 and H6 protons are designated by an asterisk (*).

The only residue in the d(A1-A2-C3-G4) single-strand region of the 13/9-mer which has an unassigned imino proton is dG4. This imino proton would be expected to be broad and upfield-shifted since dG4 lacks a partner base on the complementary strand. We do detect broad exchangeable resonances between 10.4 and 11.2 ppm (Figure 1A), and one of these could be the imino proton of dG4 in the control 13/9-mer.

Nonexchangeable Protons in the Control 13/9-Mer. All the base and sugar proton resonances, except those belonging to superpositioned sugar H5′, H5″ protons, have been assigned following analysis of NOESY, phase-sensitive COSY, and TOCSY experiments on the control 13/9-mer in D_2O buffer, pH 7.0, at 25 °C using standard assignment procedures (Hare et al., 1983). The nonexchangeable proton NMR spectrum of the base and sugar H1′ protons (5.1−8.5 ppm) of the control 13/9-mer in D_2O buffer solution, pH 7.0, at 25 °C exhibits exceptionally well resolved, narrow resonances for both the d(A1-A2-C3-G4-) single-strand and d(-C5-T6-A7- C8-C9-A10-T11-C12-C13)·d(G14- G15-A16-T17-G18-G19-T20-A21-G22) duplex segments (Figure 2A). An expanded NOESY (300 ms mixing time) contour plot correlating the pyrimidine H6 and purine H8 base protons (7.0−8.4 ppm) and the cytosine H5 and sugar H1′ protons (5.2−6.4 ppm) of the control 13/9-mer is plotted in Figure 2B. Sequential NOEs between the base protons and their own and 5′-flanking sugar H1′ protons along each chain can be readily traced from dA1 to dC13 on the 13-mer strand (solid line, Figure 2B) and from dG14 to dG22 on the 9-mer strand (dashed line, Figure 2B). The chemical shifts of the exchangeable and nonexchangeable protons centered about dG4 in the control 13/9-mer are listed in Table 1 and the complete assignments listed in the Supporting Information, Table S1.

Phosphorus Resonances in the Control 13/9-Mer. The proton-decoupled phosphorus spectrum (−3.2 to −5.0 ppm) of the control 13/9-mer in D_2O buffer at 25 °C is shown in the Supporting Information, Figure S1A. All 20 nonterminal phosphorus resonances have been assigned from an analysis of the connectivities between each phosphorus with its 5′-linked H3′ proton and 3′-linked H4′ proton in a phosphorus−proton heteronuclear correlation experiment, including the three phosphorus resonances located at the dA1-dA2, dA2-dC3, and dC3-dG4 steps on the single-strand segment (Supporting Information, Figure S1B). The phosphorus chemical shifts for the control 13/9-mer are listed in Tables 1 and S1.

Exchangeable Nucleic Acid Protons in the (+)-trans-anti-[BP]dG 13/9-Mer. The exchangeable proton NMR spectrum (9.5−14.5 ppm) of the (+)-*trans-anti*-[BP]dG 13/9-mer in H_2O buffer, pH 7.0, at 1 °C shows several partially resolved imino resonances between 12.5 and 14.0 ppm and two upfield-shifted broad resonances at 10.1 and 11.5 ppm (Figure 3A), which have been assigned following analysis of the 150 ms mixing time NOESY spectrum. The connectivities between adjacent base pairs in the 9-mer duplex

Table 1: Proton and Phosphorus Chemical Shifts of the d(A1-A2-C3-G4-C5-T6-A7)·(T20-A21-G22) Segment of the Control 13/9-Mer[a]

	G(NH1)/T(NH3)	C(NH_2-4)	H8/H6	H5/H2/CH_3	H1′	H2′	H2″	H3′	H4′	$^{31}P^b$
dA1			7.87		5.99	2.09	2.41	4.73	4.14	−4.41
dA2			8.18		6.09	2.66	2.57	4.93	4.34	−4.10
dC3			7.32	5.56	5.88	1.66	2.20	4.65	3.97	−4.24
dG4	(10.4−11.2)[c]		7.83		5.84	2.64	2.52	4.87	4.28	−3.97
dC5		7.17,[d] 8.34[e]	7.63	5.73	5.91	2.15	2.43	4.77	4.08	−4.33
dT6	13.80		7.42	1.67	5.57	2.18	2.44	4.87	4.15	−4.06
dA7			8.32	7.57	6.25	2.77	2.91	5.04	4.45	−4.30
dT20	13.69		7.19	1.36	5.56	1.95	2.27	4.82	4.13	−4.23
dA21			8.13	7.57	6.01	2.63	2.82	5.02	4.36	−4.14
dG22	12.63		7.73		5.96	2.51	2.28	4.65	4.18	

[a] All chemical shifts are in ppm. Exchangeable proton chemical shifts at 1 °C. Nonexchangeable proton and phosphorus chemical shifts at 25 °C. [b] ^{31}P chemical shift corresponds to residue n in $n - {}^{31}P - (n + 1)$ step. [c] Tentative assignment. [d] Exposed amino proton. [e] Hydrogen-bonded amino proton.

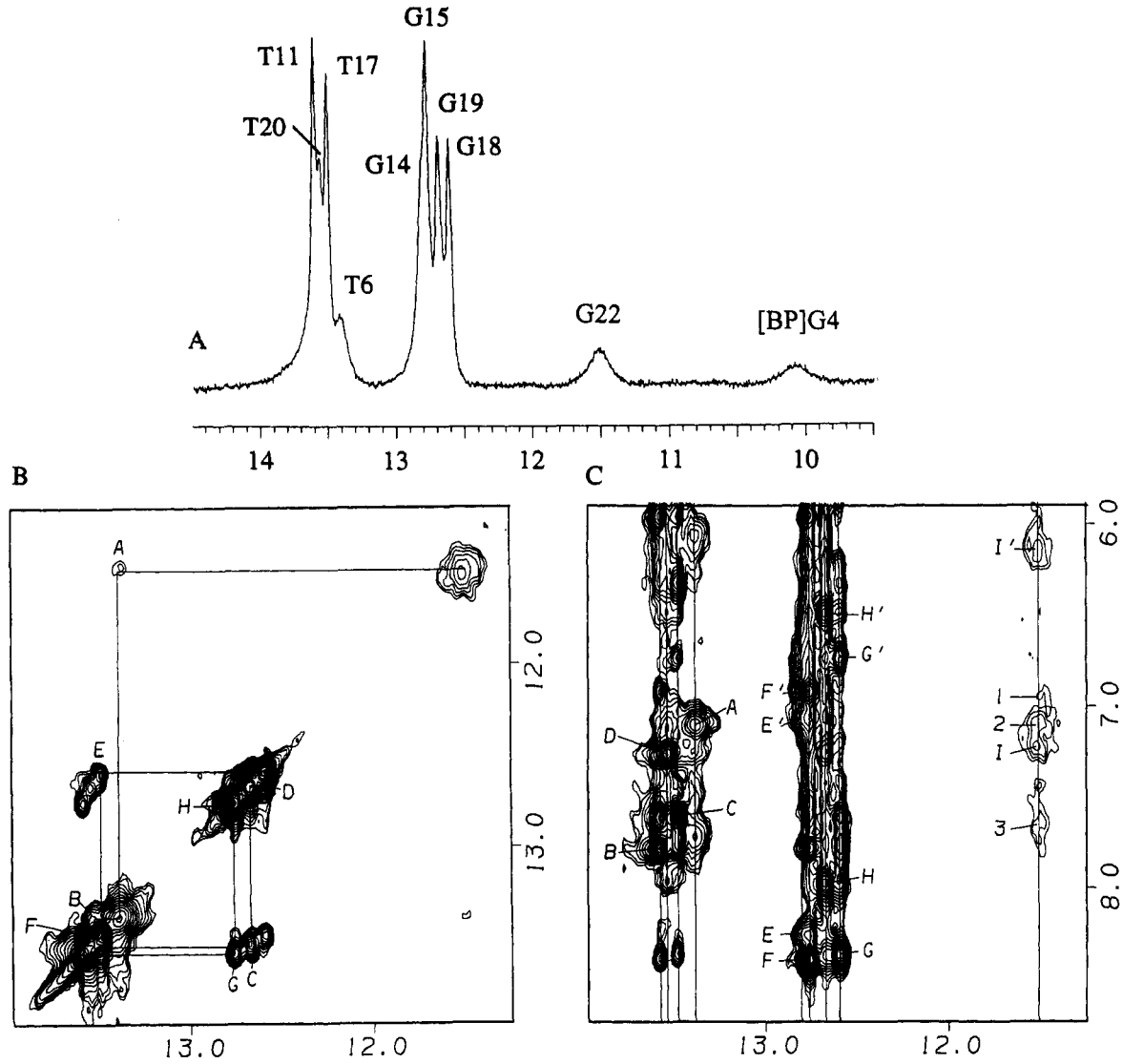

FIGURE 3: (A) Exchangeable imino proton spectrum (9.5−14.5 ppm) and (B) and (C) expanded NOESY (150 ms mixing time) contour plots of the (+)-*trans-anti*-[BP]dG 13/9-mer in H_2O buffer at 1 °C. The imino proton assignments are recorded over the spectrum in panel A. NOE connectivities between adjacent base pairs in the symmetrical 11.2−14.2 ppm region are traced in panel B, starting at dG22 located at the duplex−single strand junction site and proceeding to dG14 toward the other end of the helix. The cross peaks A−H are assigned as follows: A, dG22(NH1)-dT6(NH3); B, dT6(NH3)-dT20(NH3); C, dT20(NH3)-dG19(NH1); D, dG19(NH1)-dG18(NH1); E, dG18(NH1)-dT17(NH3); F, dT17(NH3)-dT11(NH3); G, dT11(NH3)-dG15(NH1); H, dG15(NH1)-dG14(NH1). NOE connectivities between the imino protons (11.2−14.2 ppm) and the nucleic acid base and amino protons (6.0−8.7 ppm) are designated in panel C. The cross peaks A−I′ are assigned as follows: A, dT6(NH3)-dA21(H2); B, dT11(NH3)-dA16(H2); C, dT17(NH3)-dA10(H2); D, dT20(NH3)-dA7(H2); E,E′, dG14(NH1)-dC13(NH_2-4b,e); F,F′, dG15(NH1)-dC12(NH_2-4b,e); G,G′, dG18(NH1)- dC9(NH_2-4b,e); H,H′, dG19(NH1)-dC8(NH_2-4b,e); I,I′, dG22(NH1)- dC5(NH_2-4b,e). The cross peaks identifying carcinogen−DNA NOEs in the (+)-*trans-anti*-[BP]dG 13/9-mer are numbered 1−3 in panel C and are assigned as follows: 1, BP(H5)-dG22(NH1); 2, BP(H4) and/or dA21(H2)-dG22(NH1); 3, BP(H3)-dG22(NH1).

segment can be readily traced from the dC13·dG14 pair located at one end of the helix to the dC5·dG22 pair located at the opposite end of the duplex segment adjacent to [BP]-dG4 (solid line, Figure 3B). The NOE cross peak between the broader resonances of dT6 and dG22 imino protons is very weak (peak A, Figure 3B) in the (+)-*trans-anti*-[BP]-dG 13/9-mer, similar to what was observed in the control 13/9-mer.

An expanded plot of the 150 ms mixing time NOESY spectrum of the (+)-*trans-anti*-[BP]dG 13/9-mer correlating connectivities between the imino protons (11.2−14.0 ppm) and the base and amino protons (6.0−8.7 ppm) is plotted in Figure 3C. The cross peaks involving the dC5·dG22 and dT6·dA21 base pairs of the duplex segment nearest to the [BP]dG4 residue located at the junction site are broadened upon (+)-*trans-anti*-[BP]dG adduct formation (Figure 3A). However, the Watson−Crick base-pairing alignments for these two pairs are still intact, as demonstrated by the presence of the broad cross peaks between dT6(NH3) and dA21(H2) (peak A, Figure 3C) and between dG22(NH1) and dC5(NH4-b,e) (peaks I and I′, Figure 3C). The Watson−Crick base pairing alignments for the remaining three dA·dT and four dG·dC base pairs in the 9-mer duplex segment farthest removed from the lesion site remain intact and unperturbed, as evidenced by the cross peaks between thymine imino and adenine H2 protons across the dA·dT pairs (peaks B−D, Figure 3C) and between guanine imino and cytosine amino protons across the dG·dC pairs (peaks E-H and E′-H′, Figure 3C) as well as by the lack of significant chemical shift changes for the exchangeable

protons of these residues upon (+)-*trans-anti*-[BP]dG adduct formation.

By contrast, large upfield shifts are observed for the imino proton of dG22 (−1.15 ppm) and the amino protons of dC5 (−1.10 and −1.05 for the bound and exposed protons, respectively) in the (+)-*trans-anti*-[BP]dG 13/9-mer relative to the control 13/9-mer. In addition, small to moderate upfield shifts are observed for the imino proton of dT6 (-0.14 ppm) and the base H2 proton of dA21 (−0.41 ppm).

The remaining upfield-shifted broad resonance at ~10.1 ppm has been tentatively assigned to the imino proton of [BP]dG4 since this residue lacks a complementary base to pair with on the partner strand. The exchangeable protons at ~10.1 and 11.5 ppm in the (+)-*trans-anti*-[BP]dG 13/9-mer broadened further on lowering the pH from 7.0 to 5.7.

Nonexchangeable Nucleic Acid Protons in the (+)-trans-anti-[BP]dG 13/9-Mer. The base and sugar H1′ nonexchangeable proton spectrum region (5.1−8.5 ppm) of (+)-*trans-anti*-[BP]dG 13/9-mer in D_2O buffer, pH 7.0, at 25 °C exhibits a mixture of narrow and broad resonances (Figure 4A). All the DNA base and sugar protons, with the exception of superpositioned sugar H5′, H5″ protons, have been assigned following analysis of through-space NOESY data sets (50 and 300 ms mixing times) and through bond TOCSY data sets (40 and 80 ms spin lock times) at three different temperatures (10, 25, and 29 °C). As the temperature decreased, the line widths of the cross peaks involving residues at or near the lesion site broadened significantly. However, obtaining spectra at three different temperatures was extremely useful in the assignment of cross peaks located near the HDO signal.

An expanded plot of the 300 ms mixing time NOESY spectrum correlating the purine H8 and pyrimidine H6 protons (6.9−8.3 ppm) to the sugar H1′ protons (5.0−6.6 ppm) of the (+)-*trans-anti*-[BP]dG 13/9-mer in D_2O buffer, pH 7.0, at 25 °C is shown in Figure 4B. The base to sugar H1′ connectivity along the modified 13-mer strand can be traced from dA1 to dC13, with a break occurring at the dC3-[BP]dG4 step (solid line, Figure 4B). By comparison, the base to sugar H1′ connectivity along the complementary 9-mer strand can be readily traced without interruption from dG14 to dG22 (dashed line, Figure 4B). The NOE cross peak between the H8 and H1′ protons of [BP]dG4 is broad but strong in both short (50 ms) and long (300 ms) mixing time NOESY data sets (see contour plot in the Supporting Information, Figure S2). A strong H8 to H1′ cross peak establishes that these protons are located close to each other in space (~2.5 Å), indicating that the glycosidic torsion angle for this modified [BP]dG4 residue adopts a *syn* orientation (Patel et al., 1982). The chemical shifts of the exchangeable and nonexchangeable protons centered about the [BP]dG4 adduct site in the (+)-*trans-anti*-[BP]dG 13/9-mer are listed in Table 2 and the complete assignments listed in the Supporting Information, Table S2.

Changes are observed in the chemical shifts values of protons located on residues at or near the lesion site upon (+)-*trans-anti*-[BP]dG adduct formation (Supporting Information, Figure S3). Moderate to large downfield shifts are observed for the H1′ (+0.68 ppm) and H2′ (+1.03 ppm) protons of [BP]dG4, while moderate upfield shifts are seen for the H1′ (−0.37 ppm) and H2″ (−0.47 ppm) protons of dA2 and H1′ (0.58 ppm) proton of dC5 (Figure S3). By

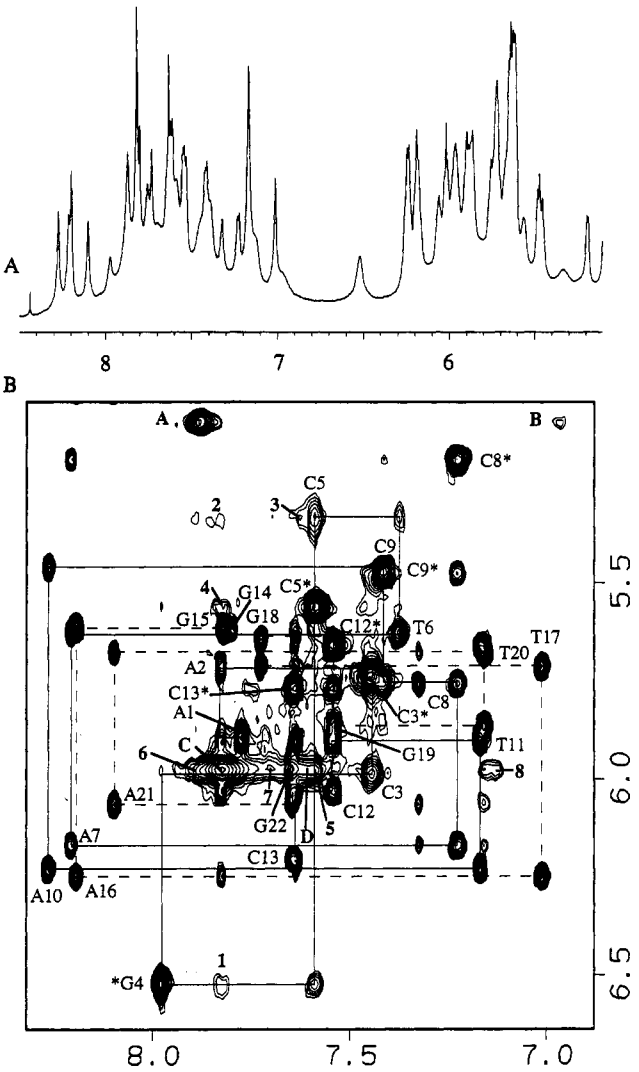

FIGURE 4: (A) Nonexchangeable proton spectrum (5.1−8.5 ppm) and (B) expanded NOESY (300 ms mixing time) contour plot of the of the (+)-*trans-anti*-[BP]dG 13/9-mer in D_2O buffer at 25 °C establishing distance connectivities between the base (purine H8 and pyrimidine H6) protons (6.9−8.3 ppm) and the sugar H1′ and cytosine H5 protons (5.0−6.6 ppm). The NOE connectivities between the base and their own and 5′-flanking sugar H1′ protons are traced from dA1 to dC13 on the template strand (solid line) and from dG14 to dG22 on the primer strand (dashed line). The cross peaks between cytosine H5 and H6 protons are designated by an asterisk (*). The cross peaks labeled A−D identify NOEs between benzo[a]pyrenyl protons and are assigned as follows: A, BP(H7)-BP(H6); B, BP(H7)-BP(H5); C, BP(H10)-BP(H11); D, BP-(H10)-BP(H12). The cross peaks numbered 1−8 identify BP-DNA NOEs and are assigned as follows: 1, [BP]dG4(H1′)-BP(H11); 2, dC5(H1′)-BP(H11); 3, dC5(H1′)-BP(H12); 4, dC5(H5)-BP(H11); 5, dC5(H6)-BP(H10); 6, dG22(H1′)-BP(H2); 7, dG22(H1′)-BP(H3); 8, dG22(H1′)-BP(H4).

contrast, no significant chemical shift changes are detected for the duplex segment located 3′ to the lesion site (Figure S3).

Phosphorus Resonances in the (+)-trans-anti-[BP]dG 13/9-Mer. The proton decoupled phosphorus spectrum (−3.2 to −5.0 ppm) of the (+)-*trans-anti*-[BP]dG 13/9-mer is shown in the Supporting Information, Figure S4A, and the resonances have been assigned after analysis of the phosphorus−proton correlation spectrum (Supporting Information, Figure S4B). The correlation between a nonterminal phosphorus and its 5′-linked H3′ proton (three-bond H−P coupling) and its 3′-linked H4′ proton (four-bond H−P

Table 2: Proton and Phosphorus Chemical Shifts of the d(A1-A2-C3-[BP]G4-C5-T6-A7)·(T20-A21-G22) Segment of the (+)-*trans-anti*-[BP]dG 13/9 Mer[a]

	G(NH1)/T(NH3)	C(NH_2-4)	H8/H6	H5/H2/CH_3	H1′	H2′	H2″	H3′	H4′	$^{31}P^b$
dA1			7.77		5.89	1.82	2.19	4.62	4.10	−4.49
dA2			7.83		5.72	2.36	2.10	4.76	4.22	−4.18
dC3			7.46	5.75	5.99	1.93	2.42	4.78	3.95	−4.02
[BP]dG4	(~10.1)[c]		7.98		6.52	3.67	2.76	4.94	4.56	−3.98
dC5		6.15,[d] 7.24[e]	7.59	5.57	5.33	1.99	2.34	4.67	4.27	−4.57
dT6	13.69		7.39	1.45	5.63	2.11	2.46	4.85	4.18	−4.25
dA7			8.22	7.32	6.18	2.66	2.85	5.00	4.41	−4.27
dT20	13.54		7.17	1.30	5.68	2.03	2.38	4.84	4.14	−4.24
dA21			8.11	7.16	6.07	2.63	2.87	5.02	4.36	−4.12
dG22	11.53		7.65		5.97	2.50	2.40	4.66	4.17	

[a] All chemical shifts are in ppm. Exchangeable proton chemical shifts at 1 °C. Nonexchangeable proton and phosphorus chemical shifts at 25 °C. [b] ^{31}P chemical shift corresponds to residue n in $n - {}^{31}P - (n + 1)$ step. [c] Tentative assignment. [d] Exposed amino proton. [e] Hydrogen-bonded amino proton.

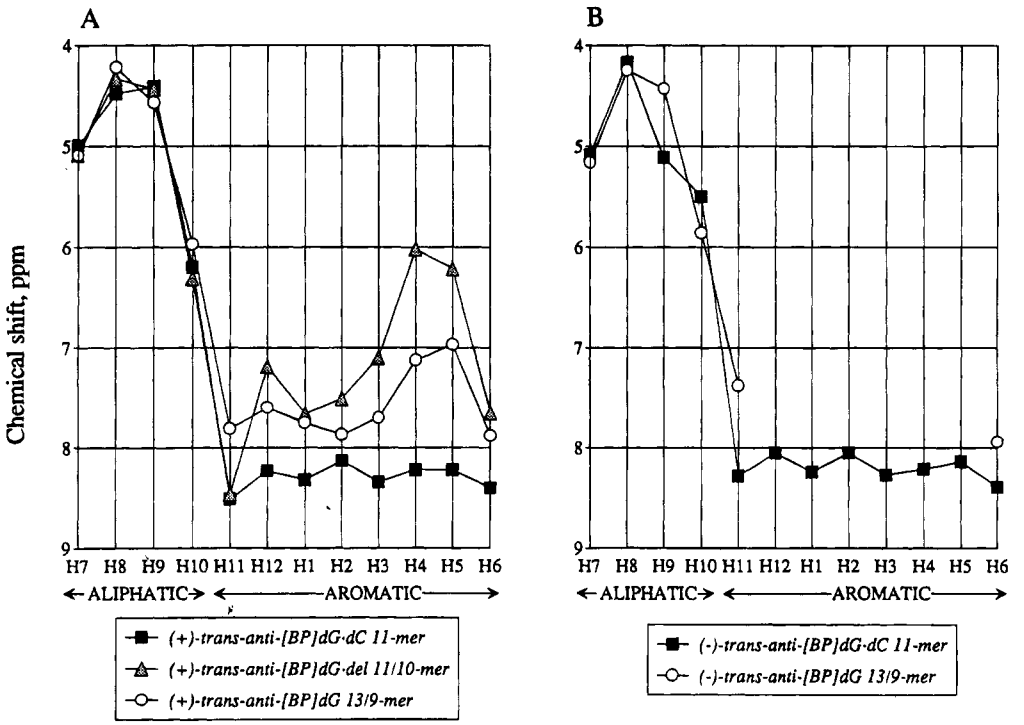

FIGURE 5: (A) Plot comparing the benzo[a]pyrenyl ring proton chemical shifts in the (+)-*trans-anti*-[BP]dG 13/9-mer, (+)-*trans-anti*-[BP]dG·dC 11-mer and (+)-*trans-anti*-[BP]dG·deletion 11/10-mer in D_2O buffer at 25 °C. The chemical shifts values in ppm for the BP protons in the (+)-*trans-anti*-[BP]dG 13/9-mer are as follows: BP(H7), 5.09; BP(H8), 4.22; BP(H9), 4.57; BP(H10), 5.97; BP(H11), 7.81; BP(H12), 7.60; BP(H1), 7.75; BP(H2), 7.87; BP(H3), 7.70; BP(H4), 7.13; BP(H5), 6.97; BP(H6), 7.88. (B) Plot comparing the benzo[a]-pyrenyl ring proton chemical shifts in the (−)-*trans-anti*-[BP]dG 13/9-mer and (−)-*trans-anti*-[BP]dG·dC 11-mer in D_2O buffer at 25 °C. The chemical shifts values in ppm for the six assigned BP protons in the (−)-*trans-anti*-[BP]dG 13/9-mer are as follows: BP(H7), 5.16; BP(H8), 4.25; BP(H9), 4.43; BP(H10), 5.86; BP(H11), 7.38.

coupling) can be followed for each phosphorus along the modified single-strand 13-mer strand, except at the dC3-[BP]-dG4 step (Figure S4B) where the 5′-dC3(H3′)-P cross peak is observed while the P-3′-[BP]dG4(H4′) cross peak is not. The phosphorus at the dC3-[BP]dG4 step is shifted downfield by +0.22 ppm, while the phosphorus at the dC5-dT6 step is shifted upfield by −0.24 ppm in the (+)-*trans-anti*-[BP]dG 13/9-mer relative to the control 13/9-mer. The phosphorus chemical shifts for the (+)-*trans-anti*-[BPdG 13/9-mer are listed in Tables 2 and S2.

Benzo[a]pyrenyl Protons in the (+)-trans-anti-[BP]dG 13/9-Mer. The chemical shifts of the nonexchangeable BP protons in the (+)-*trans-anti*-[BP]dG 13/9-mer are plotted in Figure 5A (open circles), and the values are listed in the figure caption. These protons were difficult to assign because their resonances are broad and not well resolved. The collection of NOESY and TOCSY data sets at three different temperatures (10, 25, and 29 °C) facilitated the assignment process through improvement in the resolution of severely overlapped cross peaks. The corresponding benzo[a]pyrenyl proton chemical shift values in the (+)-*trans-anti*-[BP]dG·dC 11-mer and (+)-*trans-anti*-[BP]dG·deletion 11-mer duplexes are also plotted in Figure 5A.

BP-DNA NOEs in the (+)-trans-anti-[BP]dG 13/9-Mer. A set of 23 BP-DNA NOE cross peaks, including three involving the exchangeable imino proton of dG22, have been identified in the NOESY spectra of the (+)-*trans-anti*-[BP]-dG 13/9-mer (Table 3). Several of these BP-DNA NOE cross peaks are labeled by numbers in the expanded NOESY plots of the exchangeable protons in H_2O solution (Figure 3C) and nonexchangeable protons in D_2O solution (Figure 4B). The BP-DNA crosspeak assignments are listed

Table 3: Comparison of Experimental Distance Restraints with Corresponding Distances in the Best Five Restrained Energy Minimized Structures of the (+)-*trans-anti*-[BP]dG 13/9-Mer

		distances in energy minimized structures (Å)[a]				
	restraints (Å)	no. 1	no. 2	no. 3	no. 4	no. 5
[BP]G4(H1′) to BP(H11)	2.2−6.0	4.86	4.84	4.52	4.90	4.93
[BP]G4(H2′) to BP(H10)	2.2−6.0	3.86	3.10	4.11	2.78	3.04
[BP]G4(H2′) to BP(H11)	2.2−6.0	2.61	2.60	5.12	2.44	2.65
C5(H1′) to BP(H9)	2.2−5.5	*6.05	5.42	5.39	5.47	5.24
C5(H1′) to BP(H10)	2.2−5.0	3.76	3.02	3.08	3.07	2.86
C5(H1′) to BP(H11)	2.2−5.5	3.04	*2.13	*2.13	2.37	*2.11
C5(H1′) to BP(H12)	2.2−6.0	3.26	2.67	2.73	2.90	2.83
C5(H5) to BP(H9)	2.2−5.0	4.96	4.39	4.59	4.96	5.04
C5(H5) to BP(H10)	2.2−5.0	3.99	3.73	3.77	4.14	4.11
C5(H5) to BP(H11)	2.2−6.0	5.31	5.31	5.31	5.51	5.42
C5(H6) to BP(H10)	2.2−6.0	2.58	2.41	3.00	2.85	2.67
G22(H1′) to BP(H2)	2.2−6.0	3.97	5.82	*6.07	*6.07	4.92
G22(H1′) to BP(H3)	2.2−6.0	4.08	4.55	4.44	4.77	4.46
G22(H1′) to BP(H4)	2.2−6.0	*6.12	5.34	4.47	5.59	*6.08
G22(H2″) to BP(H2)	2.2−6.0	4.52	5.64	5.65	6.00	4.92
G22(H2″) to BP(H3)	2.2−6.0	4.21	4.45	3.84	4.88	4.29
G22(H2″) to BP(H4)	2.2−6.0	*6.11	5.57	4.27	5.96	5.94
G22(H2′) to BP(H2)	2.2−6.0	5.68	5.51	*6.20	*6.04	*6.19
G22(H2′) to BP(H3)	2.2−6.0	4.78	3.72	3.97	4.29	4.99
G22(H2′) to BP(H4)	2.2−6.0	*6.14	4.32	3.38	4.77	*6.01
G22(NH1) to BP(H3)	2.2−6.0	3.94	4.28	4.73	3.90	3.73
G22(NH1) to BP(H4)	2.2−6.0	4.03	3.54	4.05	3.10	3.60
G22(NH1) to BP(H5)	2.2−6.0	4.66	3.67	3.96	3.51	4.26
$F_N + F_{NN}$ (eqs 1 and 2), $W = 30$ kcal/mol·Å^2		5.23	0.07	0.75	0.10	0.69

[a] An asterisk (*) denotes distance values which fall outside the given experimental bounds.

in the captions of Figures 3 and 4.

Most of the NOE cross peaks involving benzo[a]pyrenyl and DNA protons exhibit weak intensities. Two possible explanations for observation of a weak NOE cross peak are that either the distance between the two protons is long (4.0−5.5 Å range) or the distance between the two protons is close but one or both of the line widths of these resonances are broad. Since it was not always possible to unambiguously distinguish between these two possible explanations, the upper and lower bounds of the NMR-derived BP-DNA distance restraints were assigned wide bounds (2.2−6.0 Å) (Table 3). However, despite this uncertainty in defining the ranges for the distance restraints, the distribution of BP-DNA NOE cross peaks is consistent with only one family of orientations of the BP moiety with respect to the DNA. The C^9-C^{10}-C^{11}-C^{12} containing edge of BP is oriented toward the modified 13-mer template strand, as evidenced by the presence of NOEs between the H9, H10, H11, and H12 protons of BP and the minor and major groove base and sugar protons of [BP]dG4 and dC5 (Table 3). By contrast, the H2, H3, and H4 protons of BP located on the opposite edge of the pyrenyl ring show NOEs to the base and sugar protons of the dG22 residue, which is the 3′-terminal base of the 9-mer strand proximate to the modification site. In addition, NOEs are also observed between the H3, H4, and H5 protons of BP and the upfield shifted exchangeable imino proton of dG22 in the adduct 13/9-mer.

Exchangeable Nucleic Acid Protons in the (−)-trans-anti-[BP]dG 13/9-mer. The exchangeable proton spectrum of the (−)-*trans-anti*-[BP]dG 13/9-mer in H_2O buffer at pH 7.0 shown in Figure 6A exhibits both narrow, well-resolved resonances and numerous broad, poorly resolved resonances. We have been able to assign only the imino protons located in the d(C8-C9-A10-T11-C12-C13)·d(G14-G15-A16-T17-G18-G19) six base pair portion of the duplex segment farthest removed from the modified guanine following analysis of the 150 ms mixing time NOESY of the (−)-*trans-anti*-[BP]-dG 13/9-mer in H_2O buffer. The imino to imino connectivities between adjacent base pairs in this duplex segment can be readily traced from the dG14 residue located at one end of the helix to the dG19 residue located four base pairs away from the (−)-*trans-anti*-[BP]dG4 residue (solid line, Figure 6B). A weak cross peak observed from the dG19 imino proton to the dT20 imino proton provides a tentative assignment of the imino proton of dT20 to a broad upfield-shifted resonance at ~12.3 ppm, but it is difficult to be certain of this assignment since this resonance does not exhibit NOEs to other protons in the spectrum. The imino to imino connectivities could not be followed between the three adjacent base pairs immediately 3′ to the [BP]dG4 residue in the d(C5-T6-A7)·d(T20-A21-G22) portion of the duplex segment. In addition, more unassigned cross peaks are detected than can be accounted for by the potential assignments of the three imino protons of dT20, dT6, and dG22. This indicates conformational heterogeneity for this section of the duplex segment located immediately 3′ to the modified guanine residue in the (−)-*trans-anti*-[BP]dG 13/9-mer.

Nonexchangeable Nucleic Acid Protons in the (−)-trans-anti-[BP]dG 13/9-Mer. The nonexchangeable proton spectrum of the (−)-*trans-anti*-[BP]dG 13/9-mer in D_2O buffer, pH 7.0, exhibits narrow resonances superimposed on broad, overlapped resonances (Figure 7A). The spectrum did not improve when either the temperature of the sample was changed to values between 0 and 40 °C in 5 °C increments or when the pH of the sample was changed to ~6.0. Exchange cross peaks and very broad line widths were observed in both the NOESY and TOCSY spectra for the d(A1-A2-C3-[BP]dG4-dC5-T6)·d(A21-G22) 6/2-mer segment of the (−)-*trans-anti*-[BP]dG 13/9-mer in D_2O buffer, pH 7.0, which includes residues located within two residues on either side of the [BP]dG4 lesion site.

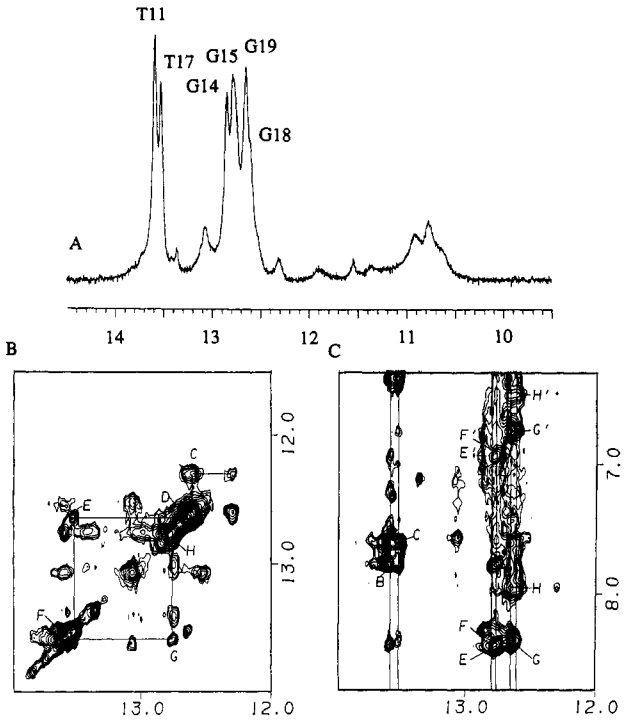

FIGURE 6: (A) Exchangeable imino proton spectrum (9.5−14.5 ppm) and (B) and (C) expanded NOESY (150 ms mixing time) contour plots of the of the (−)-*trans-anti*-[BP]dG 13/9-mer in H_2O buffer at 1 °C. The imino proton assignments are recorded over the spectrum in panel A. NOE connectivities between adjacent base pairs in the symmetrical 12.0−14.2 ppm region are traced in panel B, starting at dT20 located two base pairs away from the modified dG4 at the duplex−single strand junction site and proceeding to dG14 toward the other end of the helix. The cross peaks C to H are assigned as follows: C, dT20(NH3)-dG19(NH1); D, dG19-(NH1)-dG18(NH1); E, dG18(NH1)-dT17(NH3); F, dT17(NH3)-dT11(NH3); G, dT11(NH3)-dG15(NH1); H, dG15(NH1)-dG14-(NH1). Note that the NOE crosspeaks corresponding to A, dG22(NH1)-dT6(NH3) and B, dT6(NH3)-dT20(NH3) could not be assigned because of conformational heterogeneity of these residues. NOE connectivities between the imino protons (12.0−14.2 ppm) and the nucleic acid base and amino protons (6.0−8.7 ppm) are designated in panel C. The cross peaks B−H′ are assigned as follows: B, dT11(NH3)-dA16(H2); C, dT17(NH3)-dA10(H2); E,E′, dG14(NH1)-dC13(NH_2-4b,e); F,F′, dG15(NH1)-dC12(NH_2-4b,e); G,G′, dG18(NH1)- dC9(NH_2-4b,e); H,H′, dG19(NH1)-dC8(NH_2-4b,e). Note that the assignments of the NOE cross peaks A, dT6-(NH3)-dA21(H2), D, dT20(NH3)-dA7(H2), and I,I′, dG22(NH1)-dC5(NH_2-4b,e) involving residues located within three base pairs of the modified guanine in the (−)-*trans-anti*-[BP]dG 13/9-mer could not be assigned.

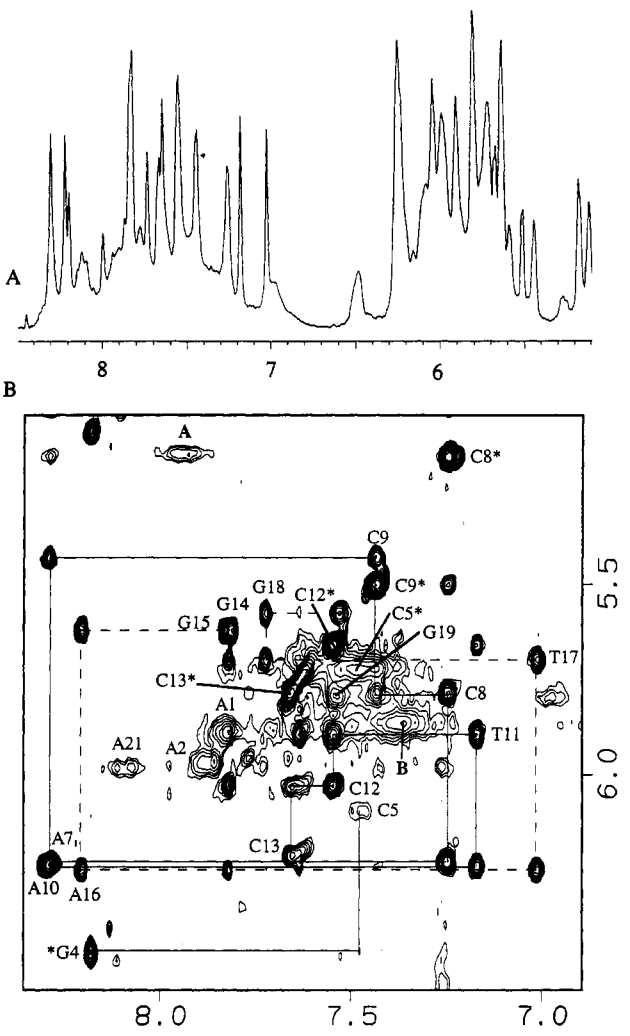

FIGURE 7: (A) Nonexchangeable proton spectrum (5.1−8.5 ppm) and (B) expanded NOESY (300 ms mixing time) contour plot of the (−)-*trans-anti*-[BP]dG 13/9-mer in D_2O buffer at 25 °C establishing distance connectivities between the base (purine H8 and pyrimidine H6) protons (6.8−8.4 ppm) and the sugar H1′ and cytosine H5 protons (5.1−6.6 ppm). The NOE connectivities between the base and their own and 5′-flanking sugar H1′ protons are traced from dA7 to dC13 on the template strand (solid line) and from dG14 to dG19 on the primer strand (dashed line). The cross peaks between cytosine H5 and H6 protons are designated by an asterisk (*). The cross peaks labeled A and B identify NOEs between benzo[a]pyrenyl protons and are assigned as follows: A, BP(H7)-BP(H6); B, BP(H10)-BP(H11).

The expanded base to H1′ region of the 300 ms NOESY spectrum of the (−)-*trans-anti*-[BP]dG 13/9-mer in D_2O buffer, pH 7.0, plotted in Figure 7B shows that the base to H1′ connectivities can be followed between dA1-dA2, [BP]-dG4-dC5, and d(A7-C8-C9-A10-T11- C12-C13) along the modified 13-mer template strand (solid lines, Figure 7B) with loss of connectivity occurring at the d(A2-C3-[BP]dG4) and d(C5-T6-A7) steps. The connectivity between the base proton and its own and flanking 5′ H1′ protons can be traced along the unmodified 9-mer primer strand (dashed line, Figure 7B) only from dG14 to the dT20 residue located three base pairs away from the modified guanine base. Although it was not possible to assign all of the exchangeable and nonexchangeable protons for the residues located at or near the lesion in the (−)-*trans-anti*-[BP]dG 13/9-mer, many assignments could still be made based on extensively cross checking the connectivities between base and sugar protons in the NOESY spectra and between the sugar protons around the deoxyribose ring in both the NOESY and TOCSY data sets. The chemical shifts (many of them tentative and enclosed in brackets) of exchangeable and nonexchangeable protons centered about the [BP]dG4 adduct site in the (−)-*trans-anti*-[BP]dG 13/9-mer are listed in Table 4 and the complete assignments listed in the Supporting Information, Table S3.

Phosphorus Resonances in the (−)-trans-anti-[BP]dG 13/9-Mer. The proton-decoupled phosphorus spectrum of the (−)-*trans-anti*-[BP]dG 13/9-mer is shown in the Supporting Information, Figure S5A. The nonterminal phosphorus resonances for the d(A7-C8-C9-A10-T11-C12-C13)•d-(G14- G15-A16-T17-G18-G19) duplex segment farthest removed from the lesion site have been assigned following analysis of the proton-phosphorus hetereonuclear correlation spectrum (Supporting Information, Figure S5B). The as-

Table 4: Proton and Phosphorus Chemical Shifts of the d(A1-A2-C3-[BP]G4-C5-T6-A7)·(T20-A21-G22) Segment of the (−)-*trans-anti*-[BP]dG 13/9-Mer (ppm)[a]

	G(NH1)/T(NH3)	C(NH_2-4)	H8/H6	H5/H2/CH_3	H1′	H2′	H2″	H3′	H4′	$^{31}P^b$
dA1			(7.83)		(5.88)					
dA2			(7.89)		(5.97)					
dC3			(7.43)	(5.72)						
[BP]dG4			(8.18)		(6.47)	(2.80)	(2.85)	(5.10)	(4.45)	
dC5			(7.62)	(5.88)						
dT6			(7.42)	(1.71)						
dA7			8.29	7.95	6.23	2.71	2.86	5.03	4.49	-4.34
dT20	(12.29)		(6.96)	(1.13)		(1.44)	(1.98)			
dA21			(8.10)	(5.98)	(5.04)	(2.58)	(2.85)	(5.04)	(4.36)	
dG22			(7.62)							

[a] All chemical shifts are in ppm. Exchangeable proton chemical shifts at 1 °C. Nonexchangeable proton and phosphorus chemical shifts at 25 °C. Tentative assignments are in brackets. [b] ^{31}P chemical shift corresponds to residue n in $n - {}^{31}P - (n + 1)$ step.

signments for these phosphorus resonances are given in the Supporting Information, Table S3. Only small chemical shift changes are observed for the phosphorus resonances in this duplex segment upon (−)-*trans-anti*-[BP]dG adduct formation relative to the control 13/9-mer. The phosphorus resonances corresponding to the d(A1-A2-C3-[BP]G4-C5-T6-A7)·d(G19-T20- A21-G22) segment located around the modification site could not be assigned because the coupling connectivities were not observed for this segment.

Benzo[a]pyrenyl Protons in the (−)-trans-anti-[BP]dG 13/9-Mer. The benzo[a]pyrenyl protons of (−)-*trans-anti*-[BP]dG4 exhibit exceedingly broad, severely overlapped resonances in the NOESY spectra (for example, see peaks A and B in Figure 7B). The eight aromatic pyrenyl protons were not observed in either the phase-sensitive COSY or the 40 and 80 ms spin lock time TOCSY spectra. By contrast, the cross peaks between the H7, H8, H9, and H10 benzylic ring protons, are observed in both TOCSY and NOESY spectra. However, exchange cross peaks involving these aliphatic protons were also observed, indicating the presence of conformational heterogeneity. In addition, the cross peaks between the aliphatic H7 proton and aromatic pyrenyl H6 proton and between the aliphatic H10 proton and aromatic pyrenyl H11 proton can be observed in the 300 ms mixing time NOESY spectrum (peaks A and B, Figure 7B). Thus, the assignments of only six of the 12 benzo[a]pyrenyl protons of the (−)-*trans-anti*-[BP]dG 13/9-mer could be made, and these assignments are plotted in Figure 5B (open circles) and listed in the figure caption. The corresponding benzo[a]pyrenyl proton chemical shift values in the (−)-*trans-anti*-[BP]dG·dC 11-mer duplex are also plotted in Figure 5B. The chemical shifts of the benzylic ring H9 proton and the two aromatic pyrenyl H11 and H6 protons of the (−)-*trans-anti*-[BP]dG 13/9-mer are upfield shifted by 0.5−1.0 ppm relative to the chemical shifts of these same protons in the (−)-*trans-anti*-[BP]dG·dC 11-mer duplex (Figure 5B).

Structural Alignment of Adduct in the (+)-trans-anti-[BP]-dG 13/9-Mer. The quality of the NMR data involving residues located at or near the lesion site in the d(A2-C3-[BP]G4-C5)·d(G22) segment of the 13/9-mer deteriorates upon (+)-*trans-anti*-[BP]dG adduct formation. The broadened line widths and associated poor cross peak resolution precludes the possibility of obtaining a high resolution structure for the (+)-*trans-anti*-[BP]dG 13/9-mer. Rather, our efforts have focused on the determination of key structural features of adduct alignment at the single strand−duplex junction. The conformational search strategy employed in the molecular mechanics program DUPLEX began with a B-DNA (Arnott et al., 1976) 9/5-mer segment of d(A1-A2-C3-[BP]G4-C5-T6-A7-C8-C9)·d(G18-G19-T20-A21-G22) from the (+)-*trans-anti*-[BP]dG 13/9-mer. In these trials the DUPLEX hydrogen-bond penalty function (Hingerty et al., 1989) for Watson−Crick base pairing was utilized at the dC5·dG22, dT6·dA21, dA7·dT20, dC8·dG19, and dC9·dG18 base pairs, since the NMR data indicated that these hydrogen bonds were present. The computations included restraints which involved both DNA-DNA [for the d(A1-A2-C3-[BP]G4-C5)·d(G22) segment] and BP-DNA interactions as well as a glycosidic torsion angle at [BP]-dG4 in the *syn* domain established experimentally. The BP-DNA orientation space was searched with 16 energy minimization trials performed on the [BP]dG 9/5-mer segment of the entire [BP]dG 13/9-mer. In these trials the linkage torsion angles α' ([BP]dG6(N^1)-[BP]dG6(C^2)-[BP]-dG6(N^2)- BP(C^{10})) and β' ([BP]dG6(C^2)-[BP]dG6(N^2)- BP-(C^{10})-BP(C^9)) were each started at 0°, 90°, 180°, and 270° in all combinations.

A view of the five structures with the best goodness-of-fit indices for eqs 1 and 2 (with $W = 30$ kcal/mol·Å^2) of the d(A1-A2-C3-[BP]G4-C5-T6-A7-C8-C9)·d(G18-G19-T20-A21-G22) segment of the (+)-*trans-anti*-[BP]dG 13/9-mer with only the duplex segments superimposed is shown in Figure 8A. The corresponding topology in a representative structure (no. 2) is shown in Figure 8B. The energy values, as well as the corresponding χ glycosidic torsion and P pseudorotation angles and linkage torsion angles α' and β' for the (+)-*trans-anti*-[BP]dG residue in each of these five structures, are given in Table 5. The goodness-of-fit values (eqs 1 and 2), which are indicative of how well the structures fit within the NMR derived BP-DNA distance restraints, are given in Table 3. The d(C5-T6-A7-C8- C9)·d(G18-G19-T20-A21-G22) duplex segment in all five of these structures adopts an unperturbed B-DNA conformation, with all base pairs maintaining Watson−Crick alignments. The [BP]dG4 residues adopt a range of conformations which exhibit the common feature that the benzo[a]pyrenyl ring stacks over the dC5·dG22 pair (Figure 8A) while the d(A1-A2-C3-) single-stranded segment is underdefined and samples a large region of conformational space (Figure 8A).

The glycosidic torsion angle χ values of the modified guanines in all five structures adopt a range of values in the *syn* domain (Table 5). It was not possible to measure three-bond vicinal proton couplings in the deoxyribose sugar ring of the [BP]dG4 residue due to large line widths of these resonances which precluded attempts to define the pucker

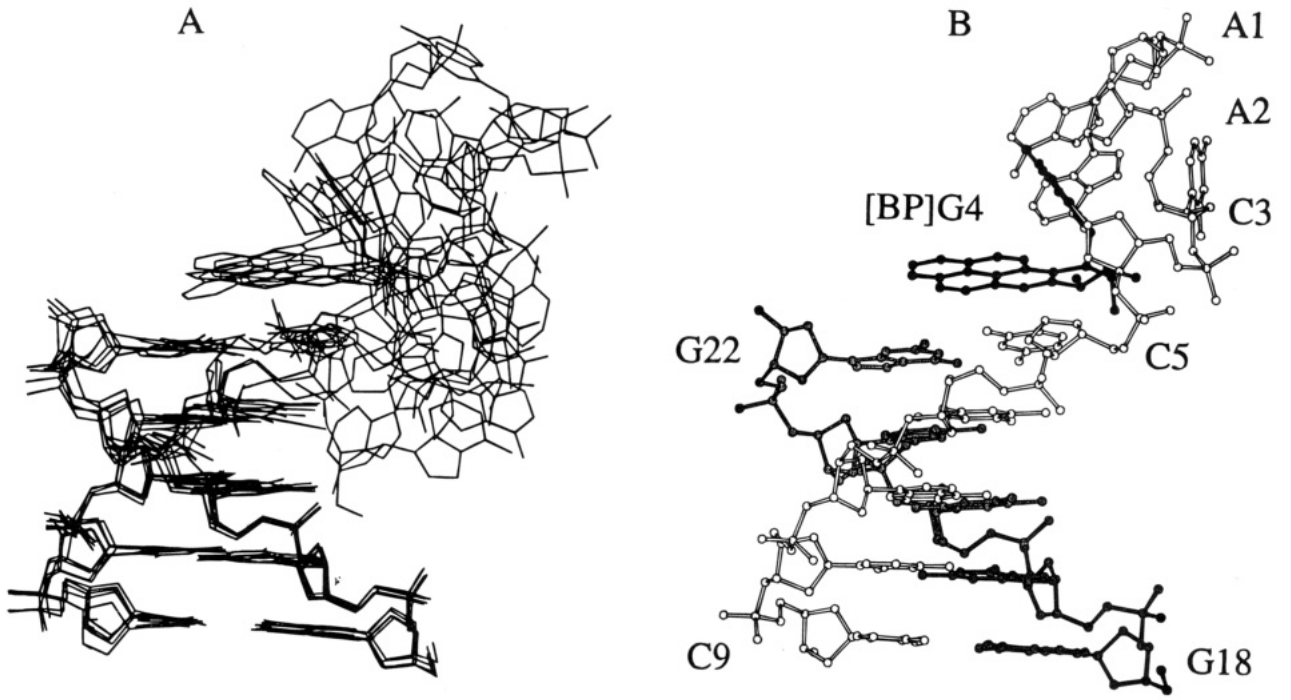

FIGURE 8: Views normal to the helix axis of the d(A1-A2-C3-[BP]G4-C5-T6-A7-C8- C9)·d(G18-G19-T20-A21-G22) 9/5-mer segment of the (+)-*trans-anti*-[BP]dG 13/9-mer. (A) Superposition of the five 9/5-mer segments that best-fit the NMR data obtained from the 16 trials to search conformational space using NMR restraints (Table 3) and the program DUPLEX. These views emphasize the conformational heterogeneity of the d(A1-A2-C3-) segment. (B) The 9/5-mer structure with the best-fit to the NMR restraints (no. 2, Table 3). The BP ring (in darkened bonds) stacks with the dC5·dG22 base pair and the *syn* [BP]dG4 base (in darkened bonds) is oriented toward the 5′ side single strand. The d(G18-G19-T20-A21-G22) primer strand (in gray bonds) and the (C5-T6-A7-C8-C9) portion of the modified template strand (in white bonds) form a minimally perturbed B-DNA duplex. The figure was prepared using Molscript V1.1 (Kraulis, 1991).

Table 5: Energy Values, the Distribution of the Sugar Pseudorotation (*P*) and Glycosidic (χ) Torsion Angles for the [BP]G4 Residue and the Linkage Site Torsion Angles α' and β'[a] for Each of the Five Calculated (+)-*trans-anti*-[BP]dG 9/5-Mer Segments

structure	energy (kcal/mol)	glycosidic angle χ ([BP]dG4)	sugar pseudorotation[b] *P* ([BP]dG4)	α'	β'
1	−309	95°	38° (C4′-exo)	281°	168°
2	−304	78°	118° (C1′-exo)	242°	203°
3	−293	161°	130° (C1′-exo)	147°	283°
4	−282	76°	183° (C3′-exo)	213°	226°
5	−282	76°	116° (C1′-exo)	237°	208°

[a] Linkage torsion angles are defined as follows: α' ([BP]dG6(N^1)-[BP]dG6(C^2)-[BP]dG6(N^2)- BP(C^{10})) and β' ([BP]dG6(C^2)-[BP]dG6(N^2)-BP(C^{10})-BP(C^9)). [b] IUPAC definition; *P* is the deoxyribose pseudorotation parameter (Altona & Sundaralingam, 1972).

of the [BP]dG4 sugar ring. The sugar pucker for [BP]dG4 adopts a range of values in the five calculated structures (Table 5).

A view emphasizing the overlap geometries between the superimposed benzo[a]pyrenyl ring and the dC5·dG22 base pair of the d([BP]G4-C5)·d(G22) segment for the five best structures is shown in Figure 9A. The corresponding ovarlap geometry in a representative structure (no. 2) is shown in Figure 9B. One edge of the benzo[a]pyrenyl ring containing the [BP]H10, [BP]H11, and [BP]H12 protons is oriented toward the modified 13-mer template strand, while the opposite edge containing the [BP]H3 and [BP]H4 protons is oriented toward the dG22 residue located on the 9-mer primer strand (Figure 9B).

The (+)-*trans-anti*-[BP]dG 9/5-mer structure with the best goodness of fit values to eqs 1 and 2 and the second lowest

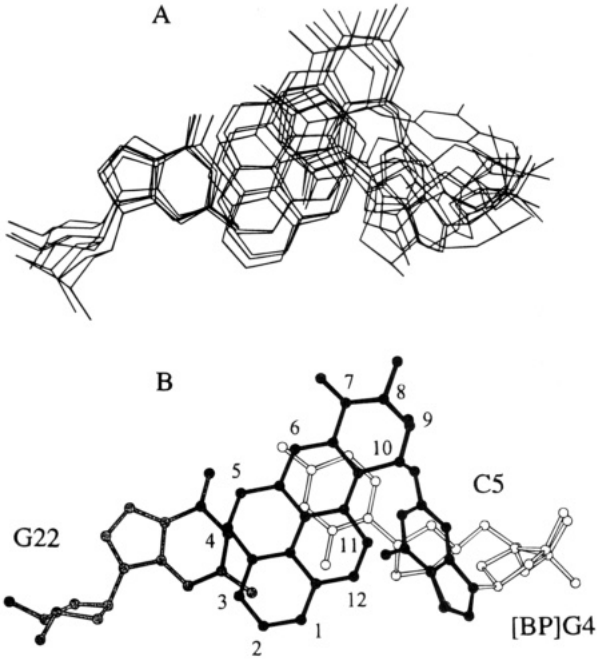

FIGURE 9: Views looking down the helix axis of the d([BP]G4-C5)·d(G22) segment of the (+)-*trans-anti*-[BP]dG 13/9-mer. (A) Superposition of the five 2/1-mer segments that best-fit the NMR restraints. (B) The 2/1-mer structure with the best-fit to the NMR restraints (no. 2, Table 3). One face of the pyrenyl ring (in darkened bonds) stacks with the dC5·dG22 base pair while the other face is solvent exposed. The figure was prepared using Molscript V1.1 (Kraulis, 1991).

energy value (no. 2, Table 5) was next built up to the 13/9-mer and minimized with all restraints. Subsequently, the hydrogen-bond penalty function and the distance restraints

were released with energy minimization in one step yielding a final unrestrained structure (Supporting Information, Figure S6C).

Structural Alignment of Adduct in the (−)-trans-anti-[BP]-dG 13/9-Mer. It was not possible to obtain structural information on the alignment of (−)-*trans-anti*-[BP]dG at the duplex−strand junction since the NMR data were characterized by very broad and overlapped cross peaks for protons located at and around the adduct site. The assignments of the BP protons were either very difficult or impossible to determine, and it was not possible to identify NOE cross peaks between the BP and nucleic acid protons. An unexpected feature is that incorporation of the (−)-*trans-anti*-[BP]dG adduct at the duplex−strand junction results in conformational heterogeneity for the flanking d(C5-T6-A7)·d(T20-A21-G22) segment which would normally adopt a duplex structure.

DISCUSSION

Spectral Quality and Information Content. Exceptionally well resolved exchangeable (Figure 1A) and nonexchangeable (Figure 2A) proton resonances are observed for the control 13/9-mer in aqueous solution. We also detect well resolved NOE connectivities involving exchangeable (Figure 1B) and nonexchangeable (Figure 2B) protons for the single strand and duplex segments in the NOESY data sets of the control 13/9-mer.

By contrast, line widths broaden for both exchangeable (Figure 3A) and nonexchangeable (Figure 4A) proton resonances of the d(A2-C3-[BP]dG4-dC5)·d(G22) segment upon formation of the (+)-*trans-anti*-[BP]dG adduct at the junction site of the single-strand and duplex regions. A series of weak and broad BP-DNA NOEs between benzo[a]pyrenyl and nucleic acid protons (numbered cross peaks in Figures 3B and 4B) were observed and provided the restraints (Table 3) necessary for alignment of the benzo[a]pyrenyl ring with respect to the dC5·dG22 base pair at the junction site. The benzo[a]pyrenyl edge containing the bay region H10 and H11 protons is directed toward dC5, while the opposite edge of the benzo[a]pyrenyl ring containing the H4 and H5 protons is directed toward dG22. Overall, the deterioration of the spectral quality upon (+)-*trans-anti*-[BP]dG adduct formation in the 13/9-mer is predominantly localized to the dA2 and dC3 single-strand residues located immediately to the 5′ side of the modified guanine, while the duplex segment located 3′ to the lesion site remains unperturbed and the benzo[a]pyrenyl ring adopts a defined orientation at the junction site relative to the proximate dC5·dG22 base pair.

The exchangeable (Figure 6) and nonexchangeable (Figure 7) proton spectra of the (−)-*trans-anti*-[BP]dG 13/9-mer exhibit a striking lack of resolution and broad line widths for the resonances located in the d(A1-A2-C3-[BP]G4-C5-T6)·d(A21-G22) segment. It was therefore not possible to make definitive proton assignments for this segment centered about the (−)-*trans-anti*-[BP]dG4 adduct site nor was it possible to identify and monitor BP-DNA NOEs for the critical d(A1-A2-C3-[BP]G4-C5-T6)·d(A21-G22) region of the (−)-*trans-anti*-[BP]dG 13/9-mer.

NOE and Chemical Shift Patterns in the (+)-trans-anti-[BP]dG 13/9-Mer. The key structural features of the five calculated structures of the (+)-*trans-anti*-[BP]dG 13/9-mer that best fit the NMR distance restraints (Figure 8) and are supported by the chemical shift data are (1) the duplex segment of the 13/9-mer located 3′ to the modified guanine remains in an unperturbed B-DNA conformation with all nine base pairs retaining Watson−Crick alignments, (2) the glycosidic torsion angle of the modified guanine adopts a *syn* orientation, (3) the benzo[a]pyrenyl ring stacks in a defined orientation with the proximate dC5·dG22 base pair located at the junction site, and (4) conformational heterogeneity detected for the d(A1-A2-C3) single-strand region located 5′ to the modified guanine.

The dC5·dG22 base pair maintains a Watson−Crick alignment as established by the presence of the cross peaks between the upfield-shifted dG22 imino proton and the amino protons of dC5 (peaks I and I′, Figure 3B). The glycosidic torsion angle values (76−161°) of the modified guanine in the five calculated structures fall within the *syn* domain. This orientation of the (+)-*trans-anti*-[BP]dG4 residue is supported by the observation of a strong NOE cross peak between the H8 base and H1′ sugar protons at short mixing times (Figure S2) and by the large downfield shifts of the H1′ and H2′ sugar protons upon adduct formation (Figure S3). By contrast, an *anti* glycosidic torsion angle is adopted by the dG4 residue in the control 13/9-mer.

The stacking interactions between the aromatic pyrenyl ring of the (+)-*trans-anti*-[BP]dG4 and the dC5·dG22 base pair (Figure 9) are supported by the large experimentally observed upfield shifts of the imino proton of dG22 (−1.15 ppm) and the amino protons of dC5 (−1.10 and −1.05 for the bound and exposed protons, respectively) on proceeding from the control 13/9-mer to the (+)-*trans-anti*-[BP]dG 13/9-mer. In addition, one face of the pyrenyl ring is stacking with the dC5·dG22 base pair, while the opposite face is solvent exposed (Figure 8), in agreement with the intermediate chemical shift values observed for the pyrenyl protons compared to the values for these protons when they are solvent exposed [(+)-*trans-anti*-[BP]dG·dC 11-mer] or sandwiched between two dG·dC base pairs [(+)-*trans-anti*-[BP]dG·deletion 11-mer] (Figure 5). The most pronounced upfield shifts are observed for the H4 and H5 protons which are positioned over the aromatic purine ring of dG22 and thus would be expected to experience the largest ring current effects (Figure 9).

The alignment of the C^9-C^{10}-C^{11}-C^{12} bay region containing edge of the BP ring toward the d(C5-[BP]G4) segment of the modified strand (Figure 9) results in the observation of NOEs between the BP(H9), BP(H10), BP(H11), and BP-(H12) protons and the base and sugar protons of dC5 and [BP]dG4 which are satisfied in the solution structures (Table 3). Moreover, the alignment of the C^3-C^4-C^5 containing edge located on the opposite side of the BP ring toward the dG22 base (Figure 9) results in the observation of NOEs between BP(H3), BP(H4), and BP(H5) protons and the imino and sugar protons of dG22 which are satisfied in the solution structures (Table 3).

The d(A1-A2-C3) segment located 5′ to the modified guanine is poorly defined consistent with the broadened line widths of the resonances involving the dA2 and dC3 protons (Figure 4A). This result suggests that (+)-*trans-anti*-[BP]-dG adduct formation at the junction site induces greater conformational heterogeneity in the single-strand region located 5′ to the modified guanine when compared with the same segment in the control 13/9-mer.

DNA Sequence Context Effects on the Structure of the (+)-trans-anti-[BP]dG Adduct. It is of interest to compare the orientations of the benzo[a]pyrenyl ring and the modified guanine base in the (+)-*trans-anti*-[BP]dG adduct in the 13/9-mer duplex−strand junction (Figures 8 and 9) with their orientations in the solution structures determined previously of the (+)-*trans-anti*- [BP]dG·dC (Cosman et al., 1992) and (+)-*trans-anti*-[BP]dG·deletion (Cosman et al., 1994) duplexes. Excellent proton NMR spectra were observed for the (+)-*trans-anti*-[BP]dG·dC 11-mer duplex in which the modified guanine is positioned opposite a cytosine base and flanked by dG·dC base pairs in the d(C5-[BP]G6-C7)·d(G16-C17-G18) sequence context (Cosman et al., 1992). A view looking into the minor groove of the solution structure of the (+)-*trans-anti*-[BP]dG·dC 11-mer duplex (Supporting Information, Figure S6A) shows that the benzo[a]pyrenyl ring (in darkened bonds) is located in a widened minor groove and is directed toward the 5′ end of the modified strand. One face of the benzo[a]pyrenyl ring is stacked over the dG18 and dA19 sugar−phosphate backbone on the partner strand and the other face is exposed to solvent. A minimally perturbed B-DNA helix is observed for the modified 11-mer duplex, with Watson−Crick alignments for all 11 base pairs including the [BP]dG6·dC17 base pair.

The proton NMR spectra observed for the (+)-*trans-anti*-[BP]dG·deletion duplex were excellent as well (Cosman et al., 1994). The modified guanine is embedded in the d(C5-[BP]G6- C7)·d(G16-G17) sequence context in a duplex containing 11 residues on the modified strand and 10 on the partner, with no base opposite the modification. A view looking into the minor groove of the solution structure of the (+)-*trans-anti*-[BP]dG·del duplex (Supporting Information, Figure S6B) shows that the benzo[a]pyrenyl ring (in darkened bonds) intercalates between intact flanking dG·dC base pairs by displacing the modified guanine base into the major groove. The displaced [BP]dG6 base is inclined relative to the DNA helix axis and stacks over the major groove base protons of the 5′-flanking dC5 residue. The intercalation site is wedge-shaped, being narrower toward the dG16-dG17 step on the deletion containing strand.

In summary, the orientations of the benzo[a]pyrenyl and modified guanine rings in the (+)-*trans-anti*-[BP]dG adduct embedded in the d(C-[BP]G-C) sequence have been studied in three different sequence environments and are strikingly different in each case. Thus, the orientation of the (+)-*trans-anti*-benzo[a]pyrenyl ring can (1) be located in the minor groove and solvent exposed when positioned opposite a cytosine (Figure S6A), (2) intercalate by displacement of the modified guanine when positioned opposite a deletion site (Figure S6B), or (3) have one face stack with the proximate dG·dC base pair and the other face solvent exposed when positioned at duplex−single strand junctions (Figure S6C). The orientation of the (+)-*trans-anti*-[BP] modified guanine can (1) maintain normal Watson−Crick base pairing alignments when it is positioned opposite a cytosine, (2) be displaced into the major groove, inclined to the helix axis, and stacked over the 5′ side cytosine base when it is positioned opposite a deletion site, or (3) adopt a *syn* glycosidic torsion angle when it is located in a junction site.

Although the conformations of the (+)-*trans-anti*-[BP]dG adduct are different in the three DNA sequence contexts outlined above, distortions in the DNA occur primarily in only one direction along the helix axis−toward the 5′ end of the modified strand in each case. The long axis of the pyrenyl ring points toward the 5′ end of the modified strand in the (+)-*trans-anti*- [BP]dG·dC 11-mer duplex, the displaced guanine is stacked over the major groove edge of the 5′ side cytosine in the (+)-*trans-anti*-[BP]dG·del duplex, and the 5′ side single-strand region exhibits conformational heterogeneity in the (+)-*trans-anti*-[BP]dG 13/9-mer single strand−duplex junction.

DNA Sequence Context Effects on the Structure of the (−)-trans-anti-[BP]dG Adduct. Excellent proton NMR spectra were observed for the (−)-*trans-anti*-[BP]dG·dC 11-mer duplex in which the modified guanine is positioned opposite a cytosine base and flanked by dG·dC base pairs (de los Santos et al., 1992). The benzo[a]pyrenyl ring is located in the minor groove and stacks with the sugar protons of the cytosine residue on the partner strand across from the modified guanine. The long axis of the pyrenyl ring is directed toward the 3′ end of the modified strand, contrasting with the results obtained with the isomeric (+)-*trans* adduct within the same sequence context in which the BP ring is oriented toward the opposite 5′-end. All 11 base pairs, including the modified [BP]dG·dC base pair, are in Watson−Crick alignments in a minimally perturbed B-DNA helix.

The quality of the proton spectra of the 13/9-mer deteriorated significantly upon (−)-*trans-anti*-[BP]dG adduct formation. This deterioration in spectral characteristics involved residues located within two to three bases of the modified guanine, including the 5′ side d(A1-A2-C3) single-strand region, the d([BP]G4-C5)·(dG22) junction site, and the 3′ side d(T6-A7-C8)·d(G19-T20-A21) portion of the duplex segment.

Consequences of (+)-trans and (−)-trans-anti-[BP]dG Adduct Stereochemistry on Structure of Duplex−Strand Junctions. (+)-*trans-anti*-[BP]dG adduct formation at a duplex−single strand junction induces conformational heterogeneity in the 5′ side d(A1-A2-C3) single-strand region, while the disorder generated by formation of the isomeric (−)-*trans-anti*- [BP]dG adduct includes regions on either side of the lesion site. Differences in directionality have been observed experimentally (Cosman et al., 1992; de los Santos et al., 1992) and predicted computationally (Singh et al., 1991) for the diametrically opposed orientations of the long axis of the pyrenyl rings in the solution structures of the (+)- and (−)-*trans-anti*-[BP]dG·dC duplex adducts. The propensity of the BP ring to either stack with nearby nucleic acid bases or be oriented in the 5′ direction for the (+)-*trans-anti*-[BP]dG adduct may account for the greater conformational heterogeneity we observe in the 5′-side single strand region in the (+)-*trans-anti*-[BP]dG template−primer sequence. The pyrenyl ring is oriented toward the 3′ end of the modified strand in the isomeric (−)-*trans* duplex adduct, and we observe considerable conformational heterogeneity in the 3′-side duplex segment nearest the modified guanine in the (−)-*trans-anti*-[BP]dG single strand−duplex junction.

The work of Mao et al. (1993) established that (+)- and (−)-*trans-anti*-[BP]dG moieties exhibit 5′ or 3′ orientations relative to the modified strand in single-stranded oligonucleotides which are similar to what has been observed at the duplex level. These orientational differences may manifest themselves on the DNA replication efficiency. We have studied the *in vitro* replication (primer extension) catalyzed by Pol I (Klenow fragment, exonuclease-free) using exactly

the same BP modified 13/9-mer sequences. The measured Michaelis−Menten kinetic parameters are less favorable for DNA replication past the (−)-*trans-anti*-[BP]dG lesion compared to the case of the stereomeric (+)-*trans-anti*-[BP]-dG adduct (Li, 1995). Further studies are required to relate the observed *in vitro* replication efficiency with the greater extent of disorder in the structure of the (−)-*trans-anti*-[BP]-dG duplex−strand junction than in that of the analogous (+)-*trans-anti*-[BP]dG 13/9-mer.

Possible Implications Regarding Interactions with Polymerases. The physical association of a polymerase with a nucleic acid substrate may involve a two-step mechanism in which the first step involves binding of the single-strand segment of the template strand in a narrow cleft of the polymerase; the polymerase then slides along the single-strand until it encounters the primer 3′-OH (Divita et al., 1993; Patel et al., 1995). Thus, the binding of a polymerase to a DNA substrate containing a (+)-*trans-anti*-[BP]dG adduct at the junction site may proceed by first having the polymerase clamp down the flexible 5′-side single-strand portion of the template strand. As the polymerase slides up toward the modified junction site, it would encounter a bulky benzo[a]pyrenyl ring stacking with the nearby template-primer base pair, and either stall temporarily or become blocked completely from making contact with the primer 3′-OH. Consequently, a structure of this type might well be responsible for the stalling and/or blockage of polymerases associated with this adduct (Mackay et al., 1992; Hruszkewycz et al., 1992; Shibutani et al., 1993; Choi et al., 1994; Moriya et al., 1995). Blockage of DNA replication by BPDE modification has been shown to be lethal to replicating mammalian cells (Wood et al., 1977).

If the polymerase bypasses the (+)-*trans-anti*-[BP] ring, the *syn* guanine could be mismatched with a residue other than a cytosine, following which extension could continue on the template strand. Incorporation of an adenine resulting in a [BP]dG(*syn*)·dA(*anti*) mismatch would ultimately result in a dG → dT transversion, providing a possible explanation for the observed prevalence of this type of point mutation produced by this adduct (Mackay et al., 1992; Shibutani et al., 1993; Moriya et al., 1995). A mismatch alignment with adenine would require conformational rearrangement of the modified guanine at the junction site. Conformational heterogeneity has been previously reported for the (+)-*cis-anti*-[BP]dG adduct opposite dC (Cosman et al., 1993a), the (+)-*trans-anti*-[BP]dG adduct opposite dC (Fountain & Krugh, 1995), and the aminofluorene-C^8 modified-dG adduct opposite dC (Eckel & Krugh, 1994) embedded in DNA oligomer duplexes. dG(*syn*)·dA(*anti*) mispairing in oligonucleotide duplexes has been demonstrated at acidic pH by NMR in solution (Gao & Patel, 1988) and X-ray in the crystalline state (Brown et al., 1989).

The single strand segment in the (+)-*trans-anti*-[BP]dG 13/9-mer exhibits considerable conformational heterogeneity (Figure 8), suggesting that the modified guanine by itself or together with the 5′-side cytosine could bulge out. Thus, the one- and two-base deletions generated by [BP]dG adducts (Shibutani et al., 1993) could result from the formation of slipped template−primer intermediates (Kunkel et al., 1990) arising when a stalled polymerase allows time for such a structural rearrangement to occur during DNA replication. In non-site-specific mutagenesis studies with (+)-*anti*-BPDE, deletions have also been observed which could arise, at least in part, from the major (+)-*trans-anti*-[BP]dG adduct (Wei et al., 1993; Rodriguez & Loechler, 1993).

The consequences of the interactions between a polymerase and a (−)-*trans-anti*-[BP]dG modified template strand would be expected to be more diverse in comparison with those of the (+)-*trans* isomer, because of the high degree of conformational heterogeneity induced around the (−)-*trans* lesion site. Although a larger variety of mutations are engendered with the (−)-*anti*-BPDE enantiomer in comparison with the (+)-enantiomer (Wei et al., 1994), this heterogeneity in the types of mutations could arise because of the known heterogeneity of adducts produced by this diol epoxide (Cheng et al., 1989) and not necessarily because of the higher degree of conformational heterogeneity of the (−)-*trans* duplex−strand junction. Moreover, Shibutani et al. (1993) did not observe mutational heterogeneity in their site-specific studies with the (−)-*trans-anti*-[BP]dG adduct. Instead, they observed a much higher frequency of dAMP insertion opposite the (−)-*trans-anti*-[BP]dG residue than with the (+)-*trans-anti*-isomer. As in the case of the (+)-*trans* adduct, the (−)-*trans-anti*-[BP]dG adduct was also found to inhibit template elongation by both T7 RNA polymerase (Choi et al., 1994) and the Klenow fragment of *E. coli* DNA polymerase I (Shibutani et al., 1993).

In conclusion, the combined NMR-molecular mechanics study of the (+)- and (−)-*trans-anti*-[BP]dG 13/9-mer duplex−strand junctions have given us some insights into the origin of the differences in the biological activities of the (+)- and (−)-*anti*-BPDE adducts. In the future, if possible, it would be of great interest to study the structural characteristics of a BP modified template−primer complexed with the DNA binding domain of a polymerase.

It should also be noted that stereoisomeric polycyclic aromatic hydrocarbon (PAH) diol epoxide adducts with the N^6 exocyclic amino group of adenine positioned opposite thymine (Cosman et al., 1993b, 1995; Schurter et al., 1995b) and guanine (Schurter et al., 1995a) have been reported in the literature. Our present structural studies on stereoisomeric BP-N^2-dG adducts at duplex−single strand junctions can be extended to their stereoisomeric PAH-N^6-dA adduct counterparts at related junctional sites.

SUPPORTING INFORMATION AVAILABLE

Three tables listing the complete exchangeable and non-exhangeable proton chemical shifts and phosphorus chemical shifts for the control, (+)-*trans-anti*-[BP]dG, and (−)-*trans-anti*-[BP]dG 13/9-mers, and six figures showing the proton-decoupled phosphorus spectra and proton−phosphorus correlation experiments of the control, (+)-*trans-anti*-[BP]dG, and (−)-*trans-anti*-[BP]dG 13/9-mers, plots of the chemical shift differences between the (+)-*trans-anti*-[BP]dG and control 13/9-mers of the minor and major groove base and sugar protons, a short mixing time NOESY contour plot of the fingerprint region of the (+)-*trans-anti*-[BP]dG 13/9-mer, and a comparative view of the solution structures of the (+)-*trans-anti*- [BP]dG·dC 11-mer duplex, the (+)-*trans-anti*-[BP]dG·deletion 11/10-mer duplex, and the (+)-*trans-anti*-[BP]dG 13/9-mer (15 pages). Ordering information is given on any current masthead page.

REFERENCES

Altona, C., & Sundaralingam, M. (1972) *J. Am. Chem. Soc. 94*, 8205−8212.

Arnott, S., Bond, P. J., Selsing, E., & Smith, P. J. (1976) *Nucleic Acids Res. 2*, 2459−2470.
Bax, A., & Subramanian, S. J. (1986) *J. Magn. Reson. 67*, 565−569.
Brookes, P., & Osborne, M. R. (1982) *Carcinogenesis 3*, 1223−1226.
Brown, T., Leonard, G. A., Booth, E. D., & Chambers, J. (1989) *J. Mol. Biol. 207*, 455−467.
Cheng, S. C., Hilton, B. D., Roman, J. M., & Dipple, A. (1989) *Chem. Res. Toxicol. 2*, 334−340.
Choi, D.-J., Marino-Alessandri, J. F., Geacintov, N. E., & Scicchitano, D. A. (1994) *Biochemistry 33*, 780−787.
Conney, A. H. (1982) *Cancer Res. 42*, 4875−4917.
Cosman, M., Ibanez, V., Geacintov, N. E., & Harvey, R. G. (1990) *Carcinogenesis 11*, 1667−1672.
Cosman, M., de los Santos, C., Fiala, R., Hingerty, B. E., Singh, S., Ibanez, V., Margulis, L., Live, D., Geacintov, N. E., Broyde, S., & Patel, D. J. (1992) *Proc. Natl. Acad. Sci. U.S.A. 89*, 1914−1918.
Cosman, M., de los Santos, C., Fiala, R., Hingerty, B. E., Ibanez, V., Luna, E., Harvey, R. G., Geacintov, N. E., Broyde, S., & Patel, D. J. (1993a) *Biochemistry 32*, 4145−4155.
Cosman, M., Fiala, R., Hingerty, B. E., Laryea, R. E., Lee, H., Harvey, R. G., Amin, S., Geacintov, N. E., Broyde, S., & Patel, D. J. (1993b) *Biochemistry 32*, 12488−12497.
Cosman, M., Fiala, R., Hingerty, B. E., Amin, S., Geacintov, N. E., Broyde, S., & Patel, D. J. (1994) *Biochemistry 33*, 11507−11517.
Cosman, M., Laryea, A., Fiala, R., Hingerty, B. E., Amin, S., Geacintov, N. E., Broyde, S., & Patel, D. J. (1995) *Biochemistry 34*, 1295−1307.
De los Santos, C., Cosman, M., Hingerty, B. E., Ibanez, V., Margulis, L., Geacintov, N. E., Broyde, S., & Patel, D. J. (1992) *Biochemistry 31*, 5245−5252.
Divita, G., Muller, B., Immendorfer, U., Gautel, M., Rittinger, K., Restle, T., & Goody, R. S. (1993) *Biochemistry 32*, 7966−7971.
Eckel, L. M., & Krugh, T. R. (1994) *Biochemistry 33*, 13611−13624.
Fountain, M. A., & Krugh, T. R. (1995) *Biochemistry 34*, 3152−3161.
Gao, X., & Patel, D. J. (1988) *J. Am. Chem. Soc. 110*, 5178−5182.
Gelboin, H. V. (1980) *Physiol. Rev. 60*, 1107−1166.
Hare, D. R., Wemmer, D. E., Chou, S. H., Drobny, G., & Reid, B R. (1983) *J. Mol. Biol. 171*, 319−336.
Hingerty, B. E., Figueroa, S., Hayden, T., & Broyde, S. (1989) *Biopolymers 28*, 1195−1222.
Hruszkewcz, A. M., Canella, K. A., Peltonen, K., Lotrappa, L., & Dipple, A., (1992) *Carcinogenesis 13*, 2347−2352.
Jeffrey, A. M., Jennette, K. W., Blobstein, S. H., Weinstein, I. B., Beland, F. A., Harvey, R. G., Kasai, H., Miura, I., & Nakanishi, K. (1976) *J. Am. Chem. Soc. 98*, 5714−5715.
Jeffrey, A. M. (1985) *Polycyclic Hydrocarbons and Carcinogenesis* (Harvey, R. G., Ed.) pp 187−208, ACS Symposium Series 283, American Chemical Society, Washington, D.C.
Kapitulnik, J., Wislocki, P. G., Levin, W., Yagi, H., Jerina, D. M., & Conney, A. H. (1978) *Cancer Res. 38*, 354−358.
Kraulis, P. J. (1991) *J. Appl. Crystallogr. 24*, 946−950.
Kunkel, T. A. (1990) *Biochemistry 29*, 8003−8011.
Levin, W., Wood, A. W., Yagi, H., Jerina, D. M., & Conney, A. H. (1976) *Proc. Natl. Acad. Sci. U.S.A. 73*, 3867−3871.
Li, B. (1995) Ph.D. Thesis, New York University.
Mackay, W., Benasutti, M., Drouin, E., & Loechler, E. L. (1992) *Carcinogenesis 13*, 1415−1425.
Mao, B., Li, B., Amin, S., Cosman, M., & Geacintov, N. E. (1993) *Biochemistry 32*, 11785−11793.
Marion, D., Ikura, M., Tschudin, R., & Bax, A. (1989) *J. Magn. Reson. 85*, 393−399.
Meehan, T., & Straub, K. (1979) *Nature 277*, 410−412.
Miller, E. C. (1978) *Cancer Res. 38*, 1479−1496.
Moriya, M., Spiegel, S., Fernandes, A., Amin, S., Liu, T.-M., Geacintov, N. E., & Grollman, A. P. (1995) *Proc. Natl. Acad. Sci. U.S.A.* (submitted).
Neidle, S, Subbiah, A., Kuroda, R., & Cooper, C. S. (1982) *Cancer Res. 42*, 3766−3768.
Osborne, M. R., Jacobs, S., Harvey, R. G., & Brooks, P. (1976) *Int. J. Cancer 1*, 362−368.
Patel, D. J., Kozlowski, S. A., Nordheim, A., & Rich, A. (1982) *Proc. Natl. Acad. Sci. U.S.A. 79*, 1413−1417.
Patel, P. H., Jacobo-Molina, A., Ding, J., Tantillo, C., Clark, A. D., Jr., Raag, R., Nanni, R. G., Huges, S. H., & Arnold, E. (1995) *Biochemistry 34*, 5351−5363.
Phillips, D. H. (1983) *Nature 303*, 468−472.
Rodriguez, H., & Loechler, E. L., (1993) *Carcinogenesis 14*, 373−383.
Schurter, E. J., Yeh, H. J. C., Sayer, J. M., Lakshman, M. K., Yagi, H., Jerina, D. M., & Gorenstein, D. G. (1995a) *Biochemistry 34*, 1364−1375.
Schurter, E. J., Sayer, J. M., Oh-Hara, T., Yeh, H. J. C., Yagi, H., Luxon, B. A., Jerina, D. M., & Gorenstein, D. G. (1995b) *Biochemistry 34*, 9009−9020.
Shapiro, R., Hingerty, B. E., & Brode, S. (1989) *J. Biomol. Struct. Dyn. 7*, 493−513.
Shibutani, S., Margulis, L. A., Geacintov, N. E., & Grollman, A. P. (1993) *Biochemistry 32*, 7531−7541.
Sims, P., & Grover, P. L. (1974) *Adv. Cancer Res. 20*, 165−275.
Sims, P., Grover, P. L., Swaisland, A., Pal, K., & Hewer, A. (1974) *Nature 252*, 326−328.
Singer, B., & Grunberger, D. (1983) *Molecular Biology of Mutagens and Carcinogens*, Plenum Press, New York.
Singh, S. B., Hingerty, B. E., Singh, U. C., Greenberg, J. P., Geacintov, N. E., & Broyde, S. (1991) *Cancer Res. 51*, 3482−3492.
Sklenar, V., Miyashiro, H., Zon, G., Miles, H. T., & Bax, A. (1986) *FEBS Lett. 208*, 94−98.
Stevens, C. W., Bouck, N., Burgess, J. A., & Fahl, W. E., (1985) *Mutat. Res. 152*, 5−14.
Taylor, E. R., & Olson, W. K. (1983) *Biopolymers 22*, 2667−2702.
van de Ven, F. J., & Hilbers, C. W. (1988) *Eur. J. Biochem. 178*, 1−38.
Wei, S.-J. C., Chang, R. L., Bhachech, N., Cui, X. X., Merkler, K. A., Wong, C.-Q., Henning, E., Yagi, H., Jerina, D. M., & Conney, A. H. (1993) *Cancer Res. 53*, 3294−3301.
Wei, S.-J. C., Chang, R. L., Henning, E. , Cui, X. X., Merkler, K. A., Wong, C.-Q., Yagi, H., Jerina, D. M., & Conney, A. H., (1994) *Carcinogenesis 15*, 1729−1735.
Weinstein, I. B., Jeffrey, A. M., Jennette, K. W., Blobstein, S. H., Harvey, R. G., Harris, C., Autrup, H., Kasai, H., & Nakanishi, K. (1976) *Science 193*, 592−595.
Wood, A. W., Chang, L. R., Lewin, W., Yagi, H. Thakker, D. R., Jerina, D., & Conney, A. H. (1977) *Biochem. Biophys. Res. Commun. 77*, 1389−1396.

BI951485K